

**BIOSYNTHESIS OF IRON AND NICKEL
NANOPARTICLES BY THE WATER VELVET
(*AZOLLA PINNATA* R.BR.)**



Ratima Janthima

**A Thesis Submitted in Partial Fulfillment of the Requirements for the
Degree of Master of Science in Environmental Biology
Suranaree University of Technology
Academic Year 2020**

ชีวสังเคราะห์ห่ออนุภาคนาโนเหล็กและนิกเกิลโดย آهنแดง
(*Azolla pinnata* R.Br.)



นางสาวรติมา จันธิมา

วิทยานิพนธ์นี้เป็นส่วนหนึ่งของการศึกษาตามหลักสูตรปริญญาวิทยาศาสตรมหาบัณฑิต
สาขาวิชาชีววิทยาสิ่งแวดล้อม
มหาวิทยาลัยเทคโนโลยีสุรนารี
ปีการศึกษา 2563

**BIOSYNTHESIS OF IRON AND NICKEL NANOPARTICLES BY THE
WATER VELVET (*AZOLLA PINNATA* R.BR.)**

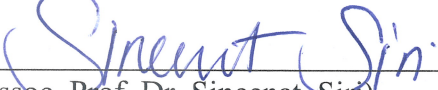
Suranaree University of Technology has approved this thesis submitted in partial fulfillment of the requirements for a Master's Degree.

Thesis Examining Committee



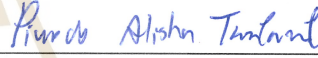
(Asst. Prof. Dr. Duangkamol Maensiri)

Chairperson




(Assoc. Prof. Dr. Sineenat Siri)

Member (Thesis Advisor)



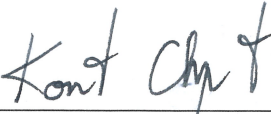
(Prof. Dr. Piyada Alisha Tantasawat)

Member

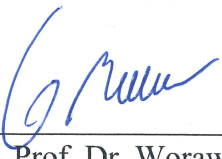


(Asst. Prof. Dr. Santi Watthana)

Member



(Assoc. Prof. Flt. Lt. Dr. Kontorn Chamniprasart)



(Assoc. Prof. Dr. Worawat Meevasana)

Vice Rector for Academic Affairs
and Internationalization

Dean of Institute of Science

รติมา จันธิมา : ชีวิตสังเคราะห์อนุภาคนาโนเหล็กและนิกเกิลโดยแหนแดง (*Azolla pinnata* R.Br.) (BIOSYNTHESIS OF IRON AND NICKEL NANOPARTICLES BY THE WATER VELVET (*AZOLLA PINNATA* R.BR.)) อาจารย์ที่ปรึกษา : รองศาสตราจารย์ ดร. สินีนาฏ ศิริ, 69 หน้า.

อนุภาคนาโนโลหะได้รับความสนใจด้านวิจัยอย่างมาก โดยเฉพาะอย่างยิ่งอนุภาคนาโนแม่เหล็กเนื่องจากคุณสมบัติและประโยชน์ในการประยุกต์ใช้ แต่อย่างไรก็ดี ยังมีการศึกษาถึงการสังเคราะห์อนุภาคนาโนแม่เหล็กในสิ่งมีชีวิตค่อนข้างน้อย โดยเฉพาะอย่างยิ่งในพืช แม้ว่าพืชหลายชนิดจัดเป็นพืชสะสมโลหะ (metal-hyperaccumulators) ซึ่งสามารถดูดซึมและกักเก็บอออนโลหะได้สูง ดังนั้นในการศึกษานี้จึงตรวจสอบความสามารถในการสังเคราะห์อนุภาคนาโนเหล็กและนิกเกิลจากอออนเหล็กและนิกเกิลที่ถูกดูดซึมโดยแหนแดง (*Azolla pinnata* R.Br.) ซึ่งเป็นเฟิร์นน้ำชนิดหนึ่งในกลุ่มพืชสะสมโลหะ ทั้งนี้จากการศึกษาความเป็นพิษของอออนเหล็กและนิกเกิลทั้งแบบเดี่ยวและผสมโดยวิเคราะห์จากการเปลี่ยนแปลงลักษณะทางสัณฐานวิทยาของใบ พบว่าโลหะทั้งสองชนิดมีความเป็นพิษต่อพืชแบบแปรผันตามความเข้มข้น และในพืชที่ได้รับโลหะทั้งสองชนิดร่วมกัน พบว่ามีผลความเป็นพิษแบบร่วมกัน จากการศึกษาด้วยเทคนิคการเรืองแสงของรังสีเอ็กซ์ในพืชที่ได้รับสารละลาย Fe^{3+} และ Ni^{2+} ที่ความเข้มข้น 50 มิลลิโมลาร์ ซึ่งพบว่ามีการดูดซึมของโลหะทั้งสองในปริมาณสูงในรากและต้น จากการวิเคราะห์ระดับโมเลกุลด้วยเทคนิคอินฟราเรดสเปกโทรสโกปีในพืชที่ได้รับโลหะ พบการเปลี่ยนแปลงการสั่นของหมู่ฟังก์ชัน ซึ่งแสดงถึงการเปลี่ยนแปลงของคาร์โบไฮเดรต โปรตีน และกรดนิวคลีอิก ที่เป็นการตอบสนองต่อโลหะของพืช นอกจากนี้ในการศึกษากิจกรรมของเอนไซม์ต้านอนุมูลอิสระ (ซูเปอร์ออกไซด์ ดิสมิวเทส คตะเลส และกลูตาไธโอนรีดักเตส) พบว่ามีการเพิ่มขึ้นของกิจกรรมของเอนไซม์ดังกล่าวซึ่งพบสูงที่สุดในพืชที่ได้รับเหล็ก รองลงมาคือเหล็กร่วมกับนิกเกิล และนิกเกิล จากการใช้กล้องจุลทรรศน์อิเล็กตรอนแบบส่องกราด ได้ภาพอนุภาคนาโนเหล็กที่เกิดขึ้นในรากพืช แต่ไม่พบอนุภาคนาโนนิกเกิล โดยอนุภาคนาโนเหล็กนี้ได้ถูกบ่งชี้ว่าอยู่ในรูปฮีมาไทต์ ($\alpha-Fe_2O_3$) และแมกนีไทต์ (Fe_3O_4) อนุภาคนาโนเหล็กเหล่านี้ถูกพบในเวสิเคิลและมัดดีเวสซิควิลาร์ บอดี หรือกระจายตัวใกล้กับเยื่อหุ้มเซลล์ในเซลล์คอร์เทกซ์และเซลล์ท่อลำเลียง ทั้งนี้เนื่องจากไม่พบการเกิดอนุภาคนาโนนิกเกิล จึงได้ใช้เทคนิคสเปกโทรเมตรีรังสีเอ็กซ์แบบกระจายพลังงานวิเคราะห์ พบว่ามีปริมาณของนิกเกิลในรากที่ระดับต่ำ จึงคาดว่ากรณีที่ไม่มีอนุภาคนาโนนิกเกิลในรากเนื่องจากความเข้มข้นของนิกเกิลที่ไม่เพียงพอต่อการชักนำให้สร้างอนุภาคนาโน ผลจากการศึกษานี้ทั้งหมดได้แสดงถึงการตอบสนองของแหนแดงต่อเหล็กและนิกเกิล และการผลิตอนุภาคนาโนเหล็กออกไซด์ในระดับ

เซลล์จากอ็อนเหล็กที่ถูกดูดซึม นอกจากนี้ ผลการทดลองนี้ยังได้ให้ความกระจ่างในข้อมูลบางประการเกี่ยวกับการตอบสนองของพืชต่อสภาวะเครียดจากโลหะ โดยเฉพาะอย่างยิ่งการเกิดอนุภาคนาโนโลหะจากอ็อนของโลหะสะสมในปริมาณสูง



สาขาวิชาชีววิทยา
ปีการศึกษา 2563

ลายมือชื่อนักศึกษา จิณต จินต
ลายมือชื่ออาจารย์ที่ปรึกษา Sinest Sili

RATIMA JANTHIMA : BIOSYNTHESIS OF IRON AND NICKEL
NANOPARTICLES BY THE WATER VELVET (*AZOLLA PINNATA* R.BR.)
THESIS ADVISOR : ASSOC. PROF. SINEENAT SIRI, Ph.D. 69 PP.

BIOSYNTHESIS/ IRON/NICKEL/NANOPARTICLES/WATER VELVET

Metal nanoparticles (MNPs), especially magnetic NPs, have received many research interests due to their outstanding properties and applications. Nevertheless, there are few studies in the biosynthesis of magnetic NPs in living organisms, especially in plants, even though several plant species are considered as metal-hyperaccumulators which can uptake and store metal ions. Therefore, in this work, the capability of water velvet (*Azolla pinnata* R.Br.), the metal-hyperaccumulator aquatic fern, was investigated for its biosynthesis of iron and nickel NPs via the uptake Fe^{3+} and Ni^{2+} ions. The toxicity of single and combination of Fe^{3+} and Ni^{2+} ions was analyzed by the morphological changes of leaves which suggested that both metals were toxic to the plant in a dose-dependent manner and the additive toxicity when both metal were combined in the treatment. At 50 mM of Fe^{3+} and Ni^{2+} ions, the metal-uptakes were investigated using energy dispersive X-ray fluorescence, which indicated the high uptake levels of each metal in roots and shoots. The molecular profiles of the metal-treated plants were analyzed by Fourier transform infrared (FTIR), which revealed the changes of functional group vibrations. The FTIR results suggested the modulations of some carbohydrates, proteins, and nucleic acids of the plants in response to metal treatments. Also, the activities of some antioxidant stress-related enzymes (superoxide dismutase, catalase, and glutathione reductase) were investigated. The results showed

the increases of these enzyme activities which were the highest in the Fe-treated plants, followed by Fe/Ni-treated and Ni-treated plants. Transmission electron microscopy images revealed the formation of FeNPs but not nickel nanoparticles (NiNPs) in the plant roots, which were identified as hematite (α -Fe₂O₃) and magnetite (Fe₃O₄) forms of FeNPs. In cortical and vascular cells, FeNPs were detected in vesicles and multivesicular bodies, or individually distributed in a vicinity of the cell membranes. Due to no observation of NiNPs, the energy-dispersive X-ray spectroscopy (EDS) analysis was employed and the result revealed the low detected level of Ni in the plant roots. Thus, no formation of NiNPs was likely due to the insufficient Ni concentration to form nanoparticles in the plant roots. Taken these results together, this work demonstrated the responses of *A. pinnata* R.Br. to iron and nickel and the cellular production of iron oxide NPs from the uptake iron ions by *A. pinnata* R.Br. These results enlightened some information of the responses of the plants to metal stress, especially on the formation of metal nanoparticles from the high accumulated levels of the uptake metal ions.

School of Biology

Academic Year 2020

Student's Signature จิตร สิม

Advisor's Signature จิตร สิม

ACKNOWLEDGEMENTS

The author would like to acknowledge the funding support from the Development and Promotion of Science and Technology Talent project (DPST) scholarship.

I would like to express my deepest and sincere gratitude to my advisor Assoc. Prof. Dr. Sineenat Siri for giving me the opportunity to do research and providing invaluable guidance and suggestions in all the time of study and writing of this thesis. Also, she always supports and encourages me to overcome all struggles in my research and my life and steer in the right direction.

I would like to express my sincere gratitude and appreciation to all teachers for enlightening and inspiring me in science. I also thank all staff of the department for their valuable assistance.

I thank my fellow Siri lab members and friends in the first batch of honor program, especially in biology major, for giving me words of encouragement and sharing all the knowledge and experiences during study.

Finally, I own my special gratitude to my family – my father and brother for being the biggest source of my strength, constantly caring, and supporting me. I also

acknowledge my late mother, who has been with me in every chapter of my life and always encouraging me to pursue my dreams.

Ratima Janthima



CONTENTS

	Page
ABSTRACT IN THAI	I
ABSTRACT IN ENGLISH	III
ACKNOWLEDGEMENT	V
CONTENTS	VII
LIST OF TABLES	IX
LIST OF FIGURES	X
LIST OF ABBREVIATIONS	XII
CHAPTER	
I INTRODUCTION	1
1.1 Background	1
1.2 Research objectives	3
1.3 Scope of the study	3
II LITERATURE REVIEWS	4
2.1 Iron and iron-nickel NPs	4
2.2 Biosynthesis of iron NPs	6
2.3 The mechanism to detoxify metal ions in plants	7
2.4 The water velvet	10
2.5 Review of related studies	12

CONTENTS (Continued)

	Page
III MATERIALS AND METHODS	15
3.1 Materials	15
3.2 Toxicity of Fe(NO ₃) ₃ and Ni(NO ₃) ₂ solutions	15
3.3 Energy dispersive X-ray fluorescence analysis	16
3.4 Attenuated total reflectance-Fourier transform infrared spectroscopy analysis	17
3.5 Accumulation of NPs in <i>Azolla pinnata</i> R.Br.	17
3.6 Characterization of NPs	18
3.7 Enzyme activities	18
3.8 Statistical analysis	20
IV RESULTS AND DISCUSSION	21
4.1 Toxicity effects of Fe(NO ₃) ₃ and Ni(NO ₃) ₂ on <i>Azolla pinnata</i> R.Br.	21
4.2 Uptake of iron and nickel ions	24
4.3 Accumulation of metal NPs in <i>Azolla pinnata</i> R.Br.	31
4.4 Identity of the metal NPs	36
4.5 Changes of functional groups of biomolecules	39
4.6 Effect of iron and nickel ions on the oxidative stress enzymes	44
VII CONCLUSION	47
REFERENCES	54
CURRICULUM VITAE	69

LIST OF TABLES

Table	Page
4.1 Summary of the FTIR profiles in roots and shoots of <i>Azolla pinnata</i> R.Br. in response to metal-treatments	43
5.1 Summary of the results	52



LIST OF FIGURES

Figure	Page
2.1 Schematic representation of major functions of thiol and non-thiol compounds, and their coordination with other defense system components in metal exposed plants	8
2.2 Reaction of enzymatic antioxidant defense on scavenging free radicals and hydrogen oxide	10
2.3 Water velvet (<i>Azolla pinnata</i> R.Br.)	11
4.1 Toxicity effects of $\text{Fe}(\text{NO}_3)_3$ and $\text{Ni}(\text{NO}_3)_2$ in <i>Azolla pinnata</i> R.Br.	22
4.2 Toxicity effect of single and combination of $\text{Fe}(\text{NO}_3)_3$ and $\text{Ni}(\text{NO}_3)_2$ solutions in <i>Azolla pinnata</i> R.Br.	24
4.3 XRF mapping of metal elements in <i>Azolla pinnata</i> R.Br. treated with $\text{Fe}(\text{NO}_3)_3$ and $\text{Ni}(\text{NO}_3)_2$ solutions	27
4.4 XRF quantitative analysis of roots and shoots of metal-treated <i>Azolla pinnata</i> R.Br.	29
4.5 TEM images of cortical cells of <i>Azolla pinnata</i> R.Br. of exposed to $\text{Fe}(\text{NO}_3)_3$ and $\text{Ni}(\text{NO}_3)_2$ solutions	32
4.6 TEM images of vascular cells of <i>Azolla pinnata</i> R.Br. roots exposed to $\text{Fe}(\text{NO}_3)_3$ and $\text{Ni}(\text{NO}_3)_2$ solutions	35
4.7 SEM-EDS analysis of roots and shoots of <i>Azolla pinnata</i> R.Br. under $\text{Fe}(\text{NO}_3)_3$ and $\text{Ni}(\text{NO}_3)_2$ treated	37

LIST OF FIGURES (Continued)

Figure	Page
4.8 SAED-TEM analyses of FeNPs in cortical cells of <i>Azolla pinnata</i> R.Br. roots	39
4.9 FTIR spectra of roots and shoots of <i>Azolla pinnata</i> R.Br. in response to metal treatments	42
4.10 The activities of antioxidant enzymes in roots and shoots of <i>Azolla pinnata</i> R.Br. treated with $\text{Fe}(\text{NO}_3)_3$ and $\text{Ni}(\text{NO}_3)_2$	46
5.1 Proposed mechanism of the formation of FeNPs in <i>Azolla pinnata</i> R.Br.	52

LIST OF ABBREVIATIONS

AgNPs	Silver Nanoparticles
ATR-FTIR	Attenuated Total Reflectance Fourier Transform Infrared
AuNPs	Gold Nanoparticles
CAT	Catalase
EDXRF	Energy Dispersive X-ray Fluorescence
SEM-EDS	Scanning Electron Microscopy and Electron Diffraction X-Ray Spectrometer
FCC	Face-centered Cubic
FeNPs	Iron Nanoparticles
GPx	Glutathione Peroxidase
GR	Glutathione Reductase
GSH	Glutathione
HR-TEM	High-Resolution Transmission Electron Microscopy
IRT	Iron-regulated Transporter
JSPDS	Joint Committee on Powder Diffraction Standards
NiNPs	Nickel Nanoparticles
NRAMP	Natural Resistance Associated Macrophage Protein
NPs	Nanoparticles
PCs	Phytochelatin
ROS	Reactive Oxygen Species

LIST OF ABBREVIATIONS (Continued)

TEM-SAED	Transmission Electron Microscopy and Selected Area Electron Diffraction
SEM	Scanning Electron Microscope
SOD	Superoxide Dismutase
TEM	Transmission Electron Microscopy
ZIP	Zinc-responsive Transporter/Iron-responsive Transporter-like Protein



CHAPTER I

INTRODUCTION

1.1 Background

The interest of metal nanoparticles (NPs) is currently increasing due to their outstanding properties and various applications in fields of biomedicine, biosensor, environmental remediation, material science, and engineering. Metal nanoparticles are the metal particles with the diameter in a range of 1-100 nm, which can consist of single or more metal components to improve their properties, such as iron-palladium, iron-platinum, and iron-nickel (Akbarzadeh et al., 2012; Lu et al., 2007). Metal NPs, especially magnetic NPs, have received many research interests due to their outstanding properties including superparamagnetic behavior, biocompatibility, facile surface modification, and catalyst support (Akbarzadeh et al., 2012; Lu et al., 2007; Reddy et al., 2012; Tang and Lo, 2013). According to these properties, magnetic NPs are applied in many technological applications, such as magnetic resonance imaging (MRI), biosensors, drug carriers, protein or cell purification, and removal of environmental contaminants (Reddy et al., 2012). Moreover, composite NPs, especially iron-nickel, offer good support strength, wear resistance, and soft magnetic properties, which are useful for several industrial applications including recording heads, transformers, and magnetic shielding materials (Lovley et al., 1987; Zhang et al., 1998).

With a high demand for metal NPs, several synthesis approaches have been developed, such as co-precipitation, thermal reduction, micelle synthesis, hydrothermal synthesis, and laser pyrolysis. These methods provide a massive production of metal NPs but require high pressure, energy, temperature, and hazard reagents. For these reasons, a biosynthesis has received increasing interests as the alternative synthesis approach since they offer simple, eco-friendly, non-toxic, and cost-effective processes. The biosynthesis of metal NPs can divide into two major groups; the synthesis using extracts derived from living organisms, and the synthesis in living organisms. Most studies have reported on the use of extracts from plants, fungi, and bacteria as the reducing and capping agents for the synthesis of metal NPs (Akbarzadeh et al., 2012; Lu et al., 2007; Pattanayak and Nayak, 2013; Weng et al., 2017). In contrast, the studies of living organisms to transform metal ions to NPs are very few. Few species of bacteria were reported to uptake and transform metal ions into membrane-bound NPs (Kim et al., 2016; Park et al., 2010). Although plants have long been used for absorbing contaminated metal ions in water and soil and detoxifying these metal ions, their ability and mechanisms to transform these metal ions to NPs remain unknown. Thus, these questions are the interests of this work. With the presence of metal ion detoxifying enzymes and many biomolecules with reducing activity in plant cells, these enzymes and biomolecules are hypothesized to function as reducing and capping agents to possibly mediate the formation of metal NPs in plant cells.

The water velvet (*Azolla pinnata* R.Br.) is the fast-growing aquatic plant that previously reported for the ability to uptake heavy metal ions (Rai, 2007; Wagner, 1997) Also, the ability of this plant to transform some metal ions to NPs were previously studied in our laboratory. Therefore, it was selected as the plant model to

study the formation of iron and nickel NPs both single and composite NPs in this study. In addition, the activity of some enzymes relating to metal responses was evaluated to understand some parts of the formation mechanism of metal NPs in this plant.

Although, living organisms, especially bacteria, are known for their ability to uptake and transform metal ions to NPs, this capability of plants is still unknown. The molecules and enzymes with reducing and capping activities in plants are potentially used as the components facilitating the formation of metal NPs. Thus, this work aimed to study on the detection of metal NPs and the activity of some enzymes relating to metal responses to understand some parts of the mechanism of metal NPs formation in plants, which the water velvet is used as the study model.

1.2 Research objectives

- 1.2.1 To study the abilities of *A. pinnata* R.Br. to uptake and transform iron and nickel ions into NPs.
- 1.2.2 To analyze the metal responses in *A. pinnata* R.Br., including metal-toxicity, metal-uptake, molecular profile of functional groups, and activity of the oxidative stress-related enzymes (superoxide dismutase, catalase, glutathione reductase).

1.3 Scope of the study

This work covers the studies of the toxic effects of iron and nickel ions in *A. pinnata* R.Br., the formation and characterization of iron and nickel NPs in the plant roots, and the activity of oxidative stress-related enzymes in response to these metal exposures.

CHAPTER II

LITERATURE REVIEWS

Nanotechnology has been used in a wide range of fields and their applications have been seen in many daily life products. Among these applications, the metal NP is one of the nanomaterials receiving many interests due to their potential applications. The metal NPs refer to the metal particles with a diameter in the range of 1 to 100 nm, which their properties are generally different from bulk material. The properties of NPs have been used in the fields of catalysis, optical biosensors, removal of heavy metal ions, and medical diagnosis/therapy. It is estimated that nanotechnology's industrial value can reach \$3 trillion by 2020 and tended to increase yearly (Tran et al., 2013).

2.1 Iron and iron-nickel NPs

Iron NPs, especially ones exhibiting strong magnetic properties (magnetic nanoparticles, MNPs), have drawn many research interests due to their various applications in biomedical diagnostic and therapy (Ito et al., 2005), drug delivery (Mody et al., 2013), catalysts (Lu et al., 2007), synthetic pigments, data storage (Akbarzadeh et al., 2012), and environmental remediation (Tang and Lo, 2013). The major groups of MNPs are ferric oxide including magnetite (Fe_3O_4) and maghemite ($\gamma\text{-Fe}_2\text{O}_3$). The finite-size and surface effects of MNPs contribute the extraordinary

property, the superparamagnetic behavior, which can be used for many biological applications, such as magnetic resonance imaging (MRI), biosensors, drug carrier protein or cell purification, and removal of environmental contaminants (Reddy et al., 2012). In addition, their surface can be easily modified, thus offering biocompatible, non-toxic, and cell-targeting properties for biomedical applications as drug delivery (Laurent et al., 2008).

Because of the widespread applications of MNPs, several methods for synthesizing MNPs have been reported, which chemical and physical methods are mostly known. The most convenient and efficient chemical method is the co-precipitation technique, which synthesizes iron oxide NPs by adding the base solution to $\text{Fe}^{2+}/\text{Fe}^{3+}$ salt solutions under an inert atmosphere at room temperature. For physical methods, the thermal reduction, micelle synthesis, hydrothermal synthesis, and laser pyrolysis techniques are well-known for providing high quality and yield of MNPs (Reddy et al., 2012).

In addition to iron NPs, iron-nickel composite NPs have received many research interests for their industrial applications due to their soft magnetic and thermal expansion properties, for example, computer storages and coating agents of recording media (Gurmen et al., 2009; Moustafa and Daoush, 2007). Iron-nickel NPs provide significantly increased strength, wear resistance, and soft magnetic properties suitable for recording heads, transformers, and magnetic shielding materials. Iron-nickel NPs have been prepared by many methods such as mechanical alloying, chemical method, spray pyrolysis, film deposition, levitation melting in liquid nitrogen, and electrodeposition (Gurmen et al., 2009; Qin et al., 1999). For a chemical reaction, iron-nickel NPs are synthesized by a reduction reaction of iron and nickel salts using a

reducing agent (i.e. borohydrides and hydrazine) to reduce these ions to zero valences (Chen et al., 2009b).

2.2 Biosynthesis of iron NPs

The biosynthesis of iron NPs has received increasing interest due to their simple, eco-friendly, non-toxic, and cost-effective processes. Two major approaches are reported; the use of extracts derived from different organisms, and the use of living organisms as the bio-factory to produce iron NPs. For the use of extracts, most studies focused on the use of plant extracts as reducing and capping agents for the formation of nanoparticles. The proteins, amino acids, vitamins, flavonoids, and polysaccharides are the major reducing and capping agents in these plant extracts. The examples of plant extracts derived from different parts and species of plants to synthesize iron NPs are mango leaves, rose leaves, jasmine leaves, and coffee seeds (Pattanayak and Nayak, 2013; Singh et al., 2016).

For the use of living organisms to produce iron NPs, most works reported on some bacterial strains that were capable of forming iron NPs encapsulated in cellular vesicles, such as *Geobacter metallireducens* GS-15 and thermophilic fermentative bacterial strain TOR-39 (Lovley et al., 1987; Zhang et al., 1998). Although the ability of plants to absorb and detoxify heavy metal ions is well-known, the capability to form metal NPs has remained unclear. In some plant species, they are able to uptake and store high levels of metal ions, which are known as phytoremediation and hyperaccumulation plants (Suman et al., 2018). However, the capability of these plants to transform the uptake metal ions into NPs has remained unknown. Based on the literature search, there

are very few reports on possible metal NPs in plants. In 2004, Rodríguez et al. reported the discovery of nano-size iron oxide mineral distributing in roots and leaves of *Imperata cylindrica*, which naturally grew in the extremely acidic environment with a high content of various metals, including iron (Rodríguez et al., 2005). In 2014, Castro-Longoria and colleagues reported the presence of lead particles in the aquatic water fern, *Salvinia minima* Baker. In this study, they explored the potential application of this plant as the lead-accumulators and suggested that cellulose, lignin, and pectin are the major components to capture lead at the specific sites (Castro-Longoria et al., 2014).

2.3 The mechanism to detoxify metal ions in plants

Metals are classified into two major groups based on their functions for plant growth, which are the essential micronutrients for plant growth (Fe, Mn, Zn, Cu, Mg, Mo, and Ni) and nonessential elements with unknown biological and physiological function (Cd, Sb, Cr, Pb, As, Co, Ag, Se, and Hg). Although these metals are important to plants, their excess levels are toxic to the plants. In general, plants can retain low concentrations of metal ions but some plant species are more tolerant and store metal at a high level, known as metal-hyperaccumulation plants. These plants use the same mechanisms to detoxify the uptake toxic metals and obtain the micronutrients from the environment. Via these mechanisms, plant roots can uptake micronutrients and toxic metal ions, which involve plant-produced chelating agents, plant-induced pH changes, and plant-induced redox reactions (Jan and Parray, 2016). Plants protect themselves from the damaging effects of metal toxicity via the mechanism illustrated in Figure 2.1. When metal ions influx to the cell, the specific biomolecules such as phytochelatin (PCs), metallothioneins (MTs), organic acids, and amino acids are used to chelate

metals and to prevent toxic reactions in the cytosol. If a number of metal ions exceed the limit of the above mechanisms, the plant will suffer from the oxidative stress caused by the production of reactive oxygen species (ROS) and the inhibition of metal-dependent antioxidant enzymes. The presence of heavy metals inside cells can activate genes of metal transporters and chelating compounds by hormone signal pathways. When metal ions are high accumulated inside the cytosol, plants have to remove them in order to reduce their toxic effects by using active efflux pumps to transport and compartmentalize the ions to the tonoplast of vacuoles (Manara, 2012).

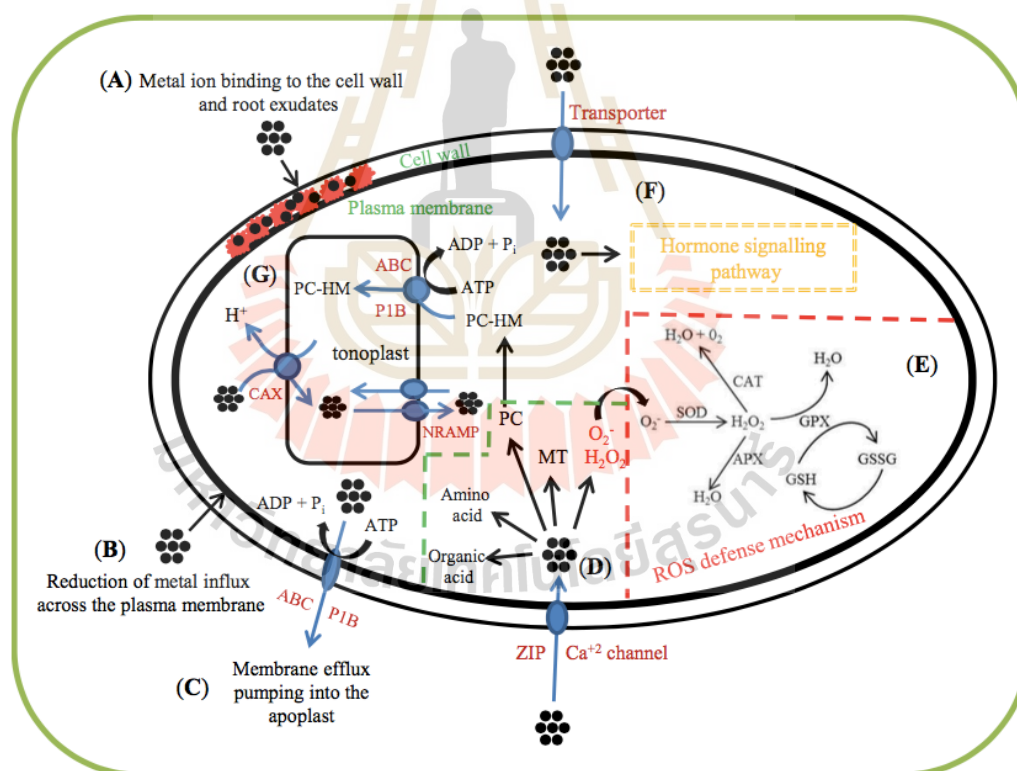


Figure 2.1 Schematic representation of major functions of thiol and non-thiol compounds, and their coordination with other defense system components in metal exposed plants (Anjum et al., 2015).

ROS were recognized as the results of abiotic stresses, including free radicals like superoxide ($O_2^{\cdot-}$) and hydroxyl (OH^{\cdot}) and non-radicals like hydrogen peroxide (H_2O_2) and singlet oxygen (1O_2). In plants, ROS were produced mostly in mitochondria and peroxisomes at basal levels, which generally derived from by-products of aerobic metabolisms. ROS production in plants were also induced by several abiotic stress conditions like salinity, heavy metals, or UV-B radiation. To cope with these stress, plants had devolved strategies to control the levels of ROS. One of these strategies was the antioxidant enzyme, such as superoxide dismutase (SOD), catalase (CAT), ascorbate peroxidase (APX), glutathione peroxidase (GPx), glutathione reductase (GR), monodehydroascorbate reductase (MDHAR), and dehydroascorbate reductase (DHAR) (Das and Roychoudhury, 2014; Szöllősi, 2014).

The first line defense antioxidants have consisted of three keys enzymes; SOD, CAT, and GPx that can breakdown ROS species to non-toxic molecules. The reactions were shown in Figure 2.2. SOD is the metalloprotein required Cu, Zn, Mn, or Fe as cofactors. SOD activity was catalyzed the transformation of the superoxide to hydrogen peroxide and oxygen. CAT is the enzyme that required Fe or Mn as a cofactor. CAT can reduce hydrogen peroxide to water and oxygen. GPx is a cytosolic enzyme that reduces hydrogen peroxide to water and oxygen by catalyzing the reduced form of glutathione. Then, the oxidized glutathione can be reversed to its reduced form by GR enzyme (Ighodaro and Akinloye, 2018; Szöllősi, 2014).

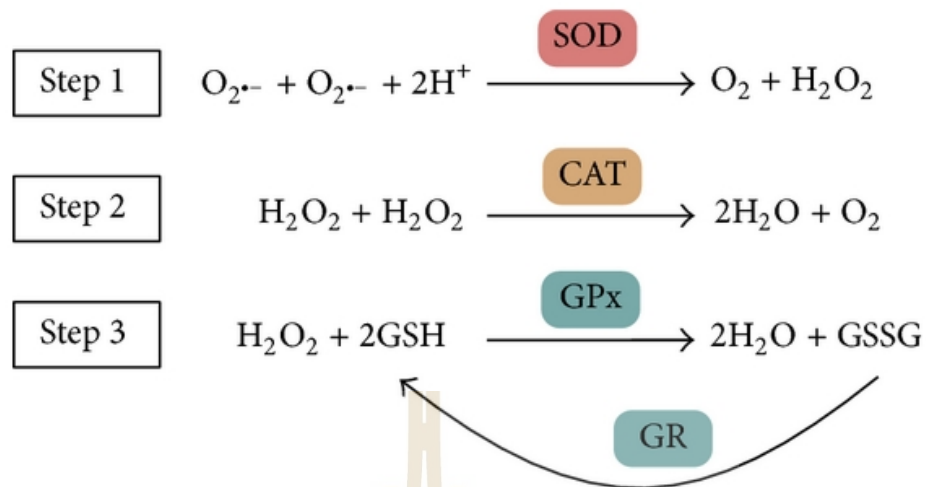


Figure 2.2 Reaction of enzymatic antioxidant defense on scavenging free radicals and hydrogen oxide. SOD, superoxide dismutase; CAT, catalase; GPx, glutathione peroxidase; and GR, glutathione reductase (Peng et al., 2014).

2.4 The water velvet

Aquatic plants are the important organisms frequently used for heavy metal uptake studies, heavy metal indicators, and biological treatments since they are widespread, eco-friendly, low cost, and toxic tolerance (Jain et al., 1990; Rai, 2007). Examples of aquatic floating plants reported for uptake some heavy metals are water hyacinth (*Eichhornia crassipes* (C. Mart.) Solms), water ferns (*Salvinia minima* Baker), duckweeds (*Lemna minor* L.), water cress (*Nasturtium officinale* W.T. Aiton) and water velvet (*Azolla pinnta* R.Br.). (Ali et al., 2020).

Azolla pinnata R.Br., known as water velvet (Figure 2.3), is one of the seven plant species in *Azolla* genus, which belongs to the family *Salviniaceae*. *A. pinnata* R.Br. has a symbiosis relationship with *Anabaena*, usually producing high productivity combined with its ability to fix nitrogen. The water velvet has been used for many applications

due to this symbiosis, such as bio-fertilizer on rice and many other crops, an animal feed, a human food, a medicine, and a water purifier (Wagner, 1997). Interestingly, five species of *Azolla* (*A. pinnata* R.Br., *A. caroliniana* Wild., *A. filiculoides* Lam., *A. microphylla* Kaulf., and *A. imbricata* (Roxb.)) are reported the potential for removing various heavy metals from contaminated water; mercury, chromium, lead, copper, zinc, uranium, manganese, cobalt, iron, and nickel (Bennicelli et al., 2004; Jain et al., 1992; Jain et al., 1989; Khosravi and Rakhshae, 2005; Sela et al., 1988; Sood et al., 2012). Therefore, *A. pinnata* R.Br. is chosen as the study model in this study.



Figure 2.3 Water velvet (*Azolla pinnata* R.Br.).

2.5 Review of related studies

As some plants efficiently remove contaminated metals from the environment, they are used as the effective approach for metal-phytoremediation. These processes are based on metal stress-tolerance mechanisms, which allow plants to survive while accumulating high concentrations of metals (Goldsbrough, 2000). Such plants, typically represented by hyperaccumulators (Baker and Brooks, 1989), have the capacity to accumulate significant amounts of metals and compartmentalize them efficiently in the cell wall, vacuole, and to the specific compartments of the cytosol in order to convert them into the nontoxic form and keep away from the important metabolic sites in plant cells (Salt et al., 1998; Memon and Schröder, 2008).

The accumulation of nanoscale metal particles in plants was first discovered in 2002, alfalfa seeds were grown on an agar medium enriched with AuCl_4 . After two weeks of growth, the formation of AuNPs were identified by XAS and TEM analyses. AuNPs were distributed in both roots and leaves of alfalfa at diameter of 2 to 20 nm. However, there was no report of the possibly biological mechanism of AuNPs formation and the specific location of this metal NPs in plant cells (Gardea-Torresdey et al., 2002).

In 2004, Benaroya et. al. reported the accumulation of Pb in *Azolla filiculoides*. After 6 days of treatment by 20 mg/L Pb^{2+} , in the Pb-treated frond, the electron-dense deposits of Pb were observed by light microscope and TEM images. Also, the elemental mass of Pb was confirmed by EDS. The electron dense of Pb was detected in vacuoles and the larger areas were found mostly inside mature leaves. Nevertheless, this work also did not purpose the possible mechanism of the formation of the Pb electron-dense,

nor confirm the crystalline structure of the Pb electron dense as metal nanoparticles (Oren Benaroya et al., 2004).

In 2014, Marchiol et al. studied the formation of AgNPs in *Brassica juncea*, *Festuca rubra*, and *Medicago sativa*. These plants were grown in the high concentration of AgNO₃ at 1,000 ppm, which the formation of AgNPs were detected by TEM and TEM X-ray microanalysis. The formation of AgNPs was discovered in roots (in cortical parenchymal cells and cell wall of the xylem vessels) and leaves (in cell wall, cytoplasm, and chloroplasts). In this work, reducing sugars and antioxidant molecules were proposed to involve the formation of NPs. Nevertheless, the crystalline structure of the formed nanoparticles did not investigate to confirm their identity (Marchiol et al., 2014).

Based on these reviews, there are still very few studies for *in vivo* biosynthesis of metal NPs from the uptake metal ions by plants. Also, the crystalline structure analysis and the possible mechanisms for the formation of metal NPs are mostly lacking. Thus, this work aimed to study the ability of *A. pinnata* R.Br. to transform the uptake iron and nickel ions into NPs as well as to characterize their crystalline structures.

CHAPTER III

MATERIALS AND METHODS

3.1 Materials

Ethylenediaminetetraacetic acid (EDTA), iron (III) nitrate ($\text{Fe}(\text{NO}_3)_3$), and nickel (II) nitrate ($\text{Ni}(\text{NO}_3)_2$) were purchased from VWR (Leuven, Belgium). Glutaraldehyde was purchased from Unilab (Auckland, New Zealand). The low viscosity embedding media Spurr's kit was purchased from Electron Microscope Science (Hatfield, PA). All other chemicals used were of analytical grade.

3.2 Toxicity of $\text{Fe}(\text{NO}_3)_3$ and $\text{Ni}(\text{NO}_3)_2$ solutions

Samples of *A. pinnata* R.Br. were collected from the botanical plant at the Suranaree University of Technology, Nakhon Ratchasima, Thailand. The collected plants were washed and incubated in deionized water for 24 h to remove any contaminated residues before being exposed to various concentrations (10–100 M) of both single and mixed solutions of $\text{Fe}(\text{NO}_3)_3$ and $\text{Ni}(\text{NO}_3)_2$ at ambient temperature for 12 h. The plant samples were then washed with 10 mM EDTA followed by deionized water to remove excesses of metallic elements from the surfaces of roots and leaves. The toxicity effects of the $\text{Fe}(\text{NO}_3)_3$ and $\text{Ni}(\text{NO}_3)_2$ solutions were calculated as the percent toxicity, which the number of damaged leaves (brown and/or withered leaves), was counted and compared with the total number of leaves.

$$\text{Toxicity (\%)} = (\text{Number of damaged leaves} / \text{Total number of leaves}) \times 100$$

3.3 Energy dispersive X-ray fluorescence analysis

To determine the uptake of iron and nickel ions, the modulation of these ions in *A. pinnata* R.Br. in response to $\text{Fe}(\text{NO}_3)_3$ and $\text{Ni}(\text{NO}_3)_2$ treatments was determined by the energy dispersive X-ray fluorescence (EDXRF) spectroscopy (Horiba Scientific, Kyoto, Japan). The *A. pinnata* R.Br. samples were treated with 50 mM $\text{Fe}(\text{NO}_3)_3$, 50 mM $\text{Ni}(\text{NO}_3)_2$, and the mixture of both solutions at ambient temperature for 12 h. Then, they were washed with 10 mM EDTA followed by deionized water to remove excesses of these solutions. The metal uptake and changes of other elemental masses inside the plants were determined by EDXRF using an X-ray analytical microscope system (Horiba Scientific, Kyoto, Japan). The analysis was carried out by using the Rh X-ray tube source, X-ray tube voltage of 50 kV, Peltier cooled silicon drift selector, and 100 s/frame count.

The accumulation of metal components was observed using the energy dispersive spectroscopy (EDS) analysis. For sample preparation, control and treated plant tissues were preserved using 2.5% glutaraldehyde in 0.1 M sodium phosphate buffer overnight and cut into 100 μm cross-section with stainless steel blade followed by dehydration in a graded series of ethanol (20–100%). Then, the plant sections were dried by vacuum drying at room temperature and attached to the stub with carbon tape. Duplicate samples of each condition were subjected to EDS spectroscopy (JEOL JSM 7800F, Tokyo, Japan) operated at 2 kV, and EDS spectra were obtained from area mapping.

3.4 Attenuated total reflectance-Fourier transform infrared spectroscopy analysis

The changes of functional groups of biomolecules in the plant roots in response to treatments were analyzed by attenuated total reflectance-Fourier transform infrared spectroscopy (ATR-FTIR) analysis. The plant samples were treated with 50 mM $\text{Fe}(\text{NO}_3)_3$, 50 mM $\text{Ni}(\text{NO}_3)_2$, and the mixture of both solutions at ambient temperature for 12 h. The excess residues of these solutions were removed by washing with 10 mM EDTA and deionized water. The IR transmission of the dried plants was recorded by a FTIR spectrometer (Bruker, Billerica, MA) in the frequency range of 400–4000 cm^{-1} . For each condition, the analysis was confirmed by performing twice using different sample sets. Spectral data were analyzed using the software system Opus 7.0 (Bruker, Billerica, MA).

3.5 Accumulation of NPs in *Azolla pinnata* R.Br.

A transmission electron microscope (TEM) was used to examine the formation of metal NPs inside the plant roots and leaves. The *A. pinnata* R.Br. samples were treated with 50 mM $\text{Fe}(\text{NO}_3)_3$, 50 mM $\text{Ni}(\text{NO}_3)_2$, and the mixture of both solutions for 12 h. After washing with 10 mM EDTA and deionized water, the plant samples were fixed in 2.5% glutaraldehyde in 0.1 M sodium phosphate buffer. Then, they were washed three times with the sodium phosphate buffer, followed by distilled water. The samples were subsequently dehydrated in acetone series (20–100%). The dried samples were embedded in a resin and polymerized at 60 °C for 48 h. Ultrathin (70–100 nm) cross-sections of the roots and leaves tissues were obtained using an ultramicrotome

PowerTome-XL (RMC Boeckeler, Tucson, AZ) with a diamond knife. Ultrathin sections were placed on bare 200 mesh copper grids and examined by transmission electron microscope (TEM; Tecnai G2 20 S-Twin, FEI, Hillsboro, OR) operating at 120 kV and the image was captured by Gatan Orius 200 CCD Camera (Gatan, Pleasanton, CA).

3.6 Characterization of NPs

To analyze the crystalline structure of the formed NPs, the ultrathin sections of the treated and control root samples were analyzed by selected area electron diffraction (SAED) using a Tecnai G2 S-Twin TEM operating at an accelerating electron source of 200 kV. In addition, the elemental composition of the synthesized nanoparticles was characterized by energy-dispersive X-ray (EDX) spectroscopy carried out on a Tecnai G2 20 S-Twin TEM equipped with an EDAX r-TEM SUTW detector (FEI, Hillsboro, OR) operating at an accelerating voltage of 15 kV.

3.7 Enzyme activities

The activities of superoxide dismutase (SOD), catalase (CAT), glutathione reductase (GR), and Fe(III) chelate reductase enzymes in response to metal treatment were evaluated. The leaves and roots of *A. pinnata* R.Br. (0.2 g fresh weight) were ground using a chilled mortar and pestle using liquid nitrogen and suspended in ice-cold homogenization buffer (phosphate buffer, 100 mM, pH 7.4). The suspensions of plant extracts were centrifuged at 10,000 g for 20 min.

The SOD activity was assayed by measuring its ability to inhibit the photochemical reduction of nitro blue tetrazolium (NBT) (Stewart and Bewley, 1980). The 2-ml

reaction consisted of 50 mM phosphate buffer (pH 7.8), 2 mM EDTA (pH 8.0), 9.9 mM L-methionine, 55 μ M NBT, and 0.025% Triton-X100. The plant extract (40 μ l) and 1 mM riboflavin (20 μ l) were added into the reaction mixture. The reaction was initiated by illuminating the samples under a 15 W fluorescent tube for 10 min in the foil-covered box. The mixtures were measured absorbance at 560 nm immediately after the reaction was stopped. One enzyme unit of SOD is defined as the amount of protein (in mg) causing a 50% inhibition of the photoreduction. The SOD activity was calculated by the equation (1).

$$\text{SOD activity} = \left(\frac{\Delta A_{\text{control}} - \Delta A_{\text{sample}}}{\Delta A_{\text{control}}} / 50\% \right) / \text{mg protein of plant extract} \quad (1)$$

The CAT activity was determined using the UV spectrophotometric method (Aebi, 1984). The reaction solution contained 10 mM H₂O₂ in 50 mM potassium phosphate buffer, pH 7.0. The reaction was carried out by adding 100 μ l plant extract to 2,900 μ l reaction solution. The decrease in absorbance at 240 nm was monitored and CAT activity was calculated by equation (2) using 40 mM⁻¹ cm⁻¹ as an absorbance coefficient (ϵ) of H₂O₂. One unit of CAT is defined as the amount of enzyme that is needed for the decomposition of 1 μ mol H₂O₂ in 1 min at 25 °C. The decrease in absorption at 240 nm was negligible in the absence of H₂O₂ or in the absence of protein extract in the reaction solution. The CAT activity was calculated by the equation (2).

$$\text{CAT activity} = \frac{\Delta A_{240} \times \text{total volume of reaction}}{\epsilon \times \text{fresh weight}} \quad (2)$$

The GR activity was assayed according to the report of Smith and colleagues (Smith et al., 1988). The increase in absorbance at 412 nm was measured when 5,5'-dithiobis(2-nitrobenzoic acid) (DTNB) was reduced to 5-thio-2-nitrobenzoic acid (TNB) by glutathione (GSH) in the reaction. In the 1-ml reaction, ten microliters of plant extract were used along with 0.75 mM DTNB and 0.1 mM NADPH. To initiate the reaction, 1 mM oxidized glutathione (GSSG) was added. The increase in absorbance was recorded every 30 s for 3 min. The extinction coefficient of TNB ($14.15 \text{ M}^{-1} \text{ cm}^{-1}$) was used to calculate the activity of GR which expressed in terms of $\text{mmole TNB min}^{-1} \text{ g}^{-1}$ (fresh weight). The GR activity was calculated by the equation (3).

$$\text{GR activity} = \frac{\Delta A_{412} \times \text{total volume of reaction}}{\epsilon \times \text{fresh weight}} \quad (3)$$

3.8 Statistical analysis

All the quantitative data were displayed as mean \pm standard deviation. The comparison of mean among groups was analyzed by one-way ANOVA and Tukey's honestly significant difference with SPSS 17.0 (Chicago, USA). P-values of less than 0.05 were considered statistically significant.

CHAPTER IV

RESULTS AND DISCUSSIONS

4.1 Toxicity effects of $\text{Fe}(\text{NO}_3)_3$ and $\text{Ni}(\text{NO}_3)_2$ on *Azolla pinnata* R.Br.

To elucidate the toxicity effects of $\text{Fe}(\text{NO}_3)_3$ and $\text{Ni}(\text{NO}_3)_2$ solutions in *A. pinnata* R.Br., the plants were exposed to various concentrations of $\text{Fe}(\text{NO}_3)_3$ and $\text{Ni}(\text{NO}_3)_2$ for 12 h. Figure 4.1(A) shows the morphological changes of leaves in response to metal exposures. In response to Fe-treatment, discolored and withered leaves were observed. Similarly, withered leaves were detected in Ni-treated plants. The corresponded % toxicity of each metal was determined and shown in Figure 4.1(B). The toxicity was increased according to the increasing concentrations of both metals. Also, $\text{Fe}(\text{NO}_3)_3$ solution was more toxic to the plants than the $\text{Ni}(\text{NO}_3)_2$ solution. As calculated via the GraphPad software, the 50% toxicity values of $\text{Fe}(\text{NO}_3)_3$ and $\text{Ni}(\text{NO}_3)_2$ solutions were 32.61 and 84.33 mM, respectively.

In principle, iron is an essential nutrient for plants that involves the electron-transport chains of photosynthesis and respiration and functions as the cofactor of many antioxidant enzymes such as Fe-SOD, catalase, ascorbate peroxidase, and guaiacol peroxidase. However, an excess amount of iron is toxic to the plants, resulting in visibly damaged morphology and even death of the plants. The obvious visual symptom in response to iron exposure is "bronzing" that is the orange-brown area on plant leaves, which caused by an accumulation of oxidized polyphenol content in leaves due to a high level of iron (Müller et al., 2015). Also, the uptake iron can cause high production

of free radicals and induce plant defending systems (Becker and Asch, 2005; Onyango et al., 2019; Sikirou et al., 2016). Similar to iron, the nickel-stress condition leads to oxidative stress, inhibition of photosynthesis, reduction of growth, inhibition of mitotic activities, and interference of other metal uptakes (Chen et al., 2009a; Yusuf et al., 2011). However, the effects of nickel on plants are generally considered less toxic (at least 100 times) to other metal trace elements as evaluated by its toxic concentration (Küpper and Andresen, 2016).

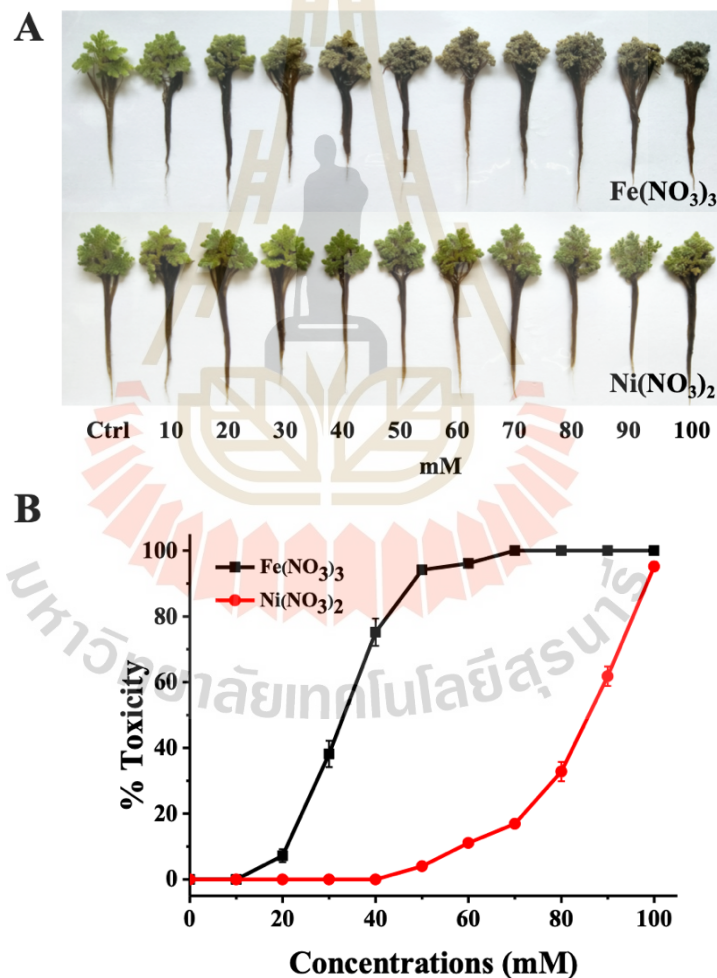


Figure 4.1 Toxicity effects of $\text{Fe}(\text{NO}_3)_3$ and $\text{Ni}(\text{NO}_3)_2$ in *Azolla pinnata* R.Br. as determined by (A) morphological changes of leaves and (B) the corresponded % toxicity.

Based on the previous experiments, the 50 mM of $\text{Fe}(\text{NO}_3)_3$ and $\text{Ni}(\text{NO}_3)_2$ caused the negative effects on *A. pinnata* R.Br.; however, at this concentration, the plants were still alive and properly functioned. Thus, this concentration was chosen for the next experiment, in which the plants were still capable to induce the cellular formation of NPs under the metal stress. Therefore, the toxicity of both solutions as single and the combination was also determined, in which the plants were treated with 50 mM $\text{Fe}(\text{NO}_3)_3$ and/or 50 mM $\text{Ni}(\text{NO}_3)_2$. The percent toxicities of 50 mM $\text{Fe}(\text{NO}_3)_3$, 50 mM $\text{Ni}(\text{NO}_3)_2$, and the mixture of both metal solutions were $94.15 \pm 0.97\%$, $4.02 \pm 0.46\%$, and $97.75 \pm 0.65\%$, respectively (Figure 4.2). The results clearly showed that at the same concentration $\text{Fe}(\text{NO}_3)_3$ was very toxic as compared with $\text{Ni}(\text{NO}_3)_2$. Also, the additive toxicity effect, not synergistic effect, was detected when both metal solutions were used to treat the plants. Although the antagonistic relationship between iron and nickel was reported as nickel competes for the uptake of iron via the inhibition of the interaction between iron and its transporters (Ghasemi et al., 2009; Shevyakova et al., 2011). In this work, the additive toxicity effect of both metals might due to the observation only the changes of leaf morphology, not the analysis of metal levels in the plants.

The toxicity effect of $\text{Fe}(\text{NO}_3)_3$ was reported to involve the formation of an oxide-hydroxide Fe^{3+} layer on the plant root, thus blocking nutrient absorption and causing nutrient deficiencies. Also, excess irons can accelerate the formation of reactive oxygen species (ROS), such as O_2^- , H_2O_2 , $^1\text{O}_2$, HO_2 , OH , OH^- , and RO , via the Fenton/Haber-Weiss reaction. These radical species can damage proteins, lipids, carbohydrates, and DNA leading to cell death (Ahmad et al., 2017). Unlike $\text{Fe}(\text{NO}_3)_3$, the toxicity of $\text{Ni}(\text{NO}_3)_2$ does not directly involve the induction of ROS (Ahmad and Ashraf, 2011).

Excess nickel in plants causes the reduction of cell division in meristematic cells and production of chlorophylls, carotenoids, total sugar, amino acids, proline, and proteins. Moreover, nickel can compete for the uptake with other essential nutrients, thus causing the nutrient deficiency in plants (Lal, 2017). Based on the effect of iron on high ROS production, it might take part in the greater toxicity of $\text{Fe}(\text{NO}_3)_3$ than $\text{Ni}(\text{NO}_3)_2$ as reported above (Gajewska and SkŁodowska, 2010; Ghasemi et al., 2009).

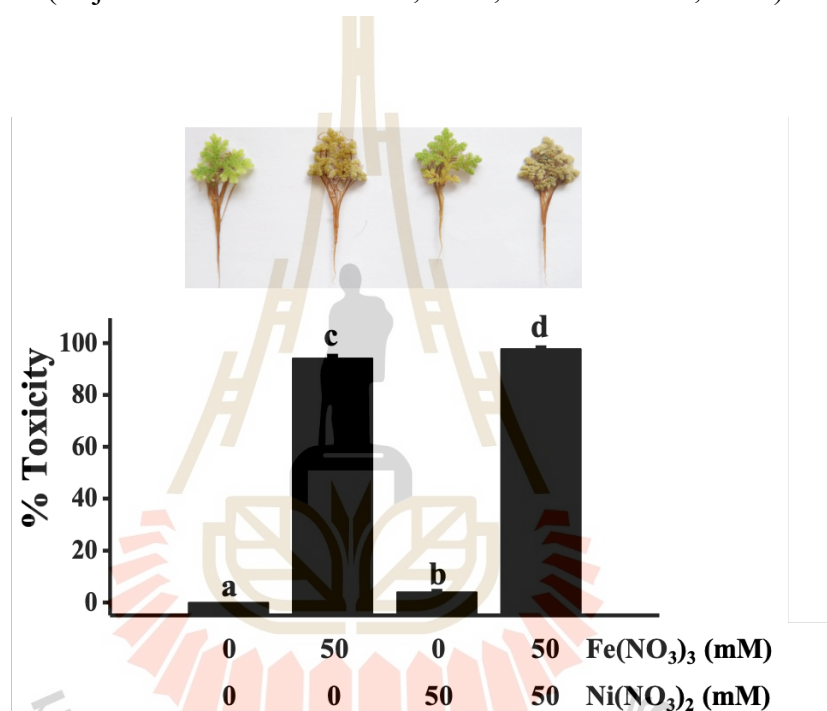


Figure 4.2 Toxicity effect of single and combination of $\text{Fe}(\text{NO}_3)_3$ and $\text{Ni}(\text{NO}_3)_2$ solutions in *Azolla pinnata* R.Br.

4.2 Uptake of iron and nickel ions

To investigate the uptake and modulation of ion levels, *A. pinnata* R.Br. treated with 50 mM $\text{Fe}(\text{NO}_3)_3$ and/or $\text{Ni}(\text{NO}_3)_2$ solutions were analyzed by EDXRF. The images of elemental mapping of *A. pinnata* R.Br. in response to metal exposure are shown in Figure 4.3. Based on thirty-one elemental analysis, there are remarkable

modulated levels of ^{17}Cl , ^{19}K , ^{20}Ca , ^{26}Fe , and ^{28}Ni . The results revealed the significant levels of ^{26}Fe and ^{28}Ni in *A. pinnata* R.Br. according to the given metal exposures but not in the control plants, suggesting that both ions were efficiently uptake and translocate to other parts of the plant.

The process of iron uptake in higher plants except those in the Graminaceae family is the reduction-based strategy, which includes three steps: acidification, reduction, and transport. If iron in the rhizosphere is in an insoluble form, it requires acidification. In this step, H^+ -ATPase pumps protons across the plasma membrane following by driving more iron into solution. On the other hand, solubilized iron may freely enter the apoplast, the cell-wall space of the outer root cell layers. In the reduction step, Fe(III) is reduced to Fe(II) mainly via an enzymatic process by the ferric chelate reductases (FRO). For the translocation step, the iron-regulated transporter (IRT1), a member of the ZIP family (zinc-regulated transporter, iron-regulated transporter-like protein) of metal transporters, and NRAMP (natural resistance-associated macrophage protein) are divalent metal transporters responsible for the transport of reduced iron across the plasma membrane into root cells (Brumbarova et al., 2015; Jeong and Connolly, 2009; Kobayashi and Nishizawa, 2012). In addition to metal transporter, iron translocation in a plant from root to shoot is also associated with appropriate chelators, such as citrate and nicotinamide (NA). Citrate in the xylem is a major chelator of iron and these Fe-citrate complexes are trafficked into xylem part via ferric reductase defective 3 (FRD3), an *Arabidopsis* transporter of the multidrug and toxic compound extrusion (MATE) family transporter FRD3. NA is a major chelator of metals in plants, which is capable to capture various transition metals, mainly Fe(II) and Fe(III) , as well as copper (Cu), nickel (Ni), cobalt (Co), manganese (Mn), and zinc (Zn) (Conte and Walker, 2011).

When iron transports into plant cells, it is distributed to required compartments for cellular activity and accumulated in some restricted area mainly in the chloroplast, mitochondrion, and vacuole to alleviate metal ion toxicity (Kobayashi and Nishizawa, 2012).

For a nickel, it is generally taken up in the plant body through the root system via passive diffusion (apoplast) and active transport (symplast) pathways depending on its concentration. Previous studies suggested that the uptake of nickel is mainly via low-affinity transport systems of the ZIP family in the plants. But no high-affinity Ni influx transporter was reported in higher plants yet (Deng et al., 2018; He et al., 2012). In the cytoplasm of root cells, nickel is rapidly complexed with organic chelators in order to decrease the toxicity, such as citrate, malate, glutamine, and NA. Moreover, some amino acids, such as histidine (His), exhibit strong nickel chelation with high affinity through the imidazole ring of nickel (Yusuf et al., 2011). Nickel is then efficiently exported from xylem parenchyma and loaded into xylem vessels, which may be due to the high expression of Ni efflux transporter(s) at parenchyma cell membranes. Once reaching leaves, the main storage organ, Ni is then transferred across the whole apoplastic space via leaf veins. Here, nickel is either absorbed by leaf cells (symplast) or remains in the apoplast (Deng et al., 2018).

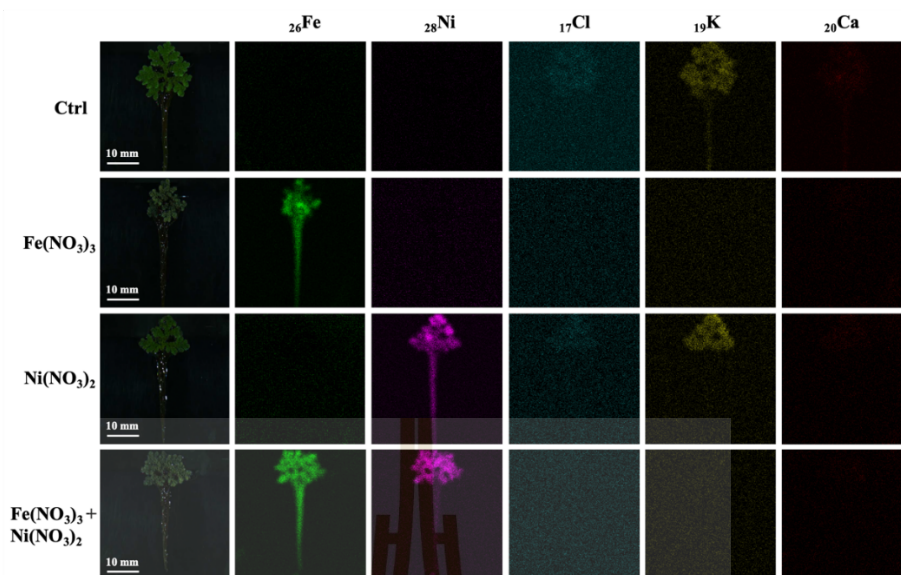
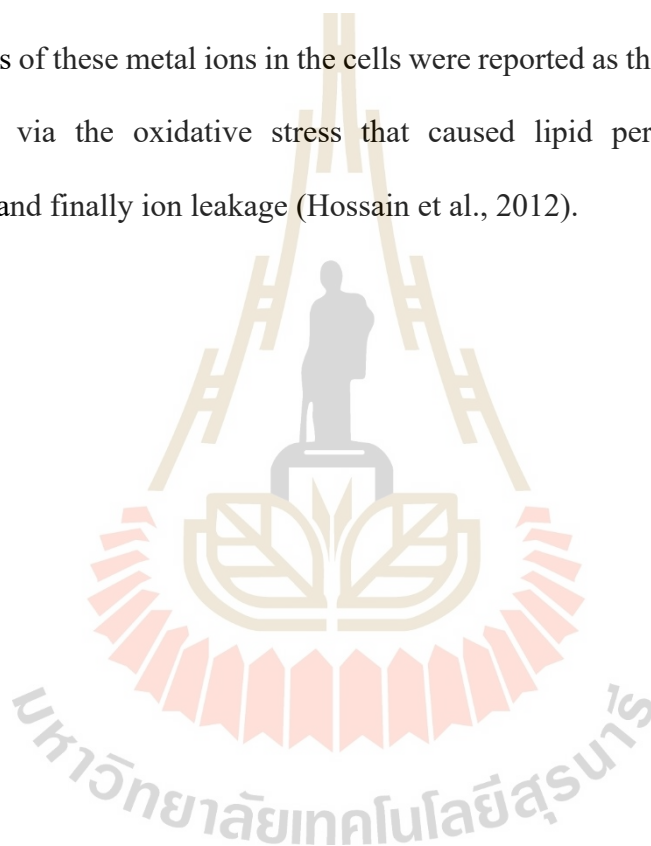


Figure 4.3 XRF mapping of ^{26}Fe , ^{28}Ni , ^{17}Cl , ^{19}K , and ^{20}Ca in *Azolla pinnata* R.Br. treated with 50 mM $\text{Fe}(\text{NO}_3)_3$ and/or $\text{Ni}(\text{NO}_3)_2$ solutions.

The corresponded levels of metal ions in the metal-treated plants are shown in Figure 4.4. In roots (Figure 4.4(A)), when *A. pinnata* R.Br. samples were treated with the combination of $\text{Fe}(\text{NO}_3)_3$ and $\text{Ni}(\text{NO}_3)_2$, the ^{26}Fe level in the plants was lower than the single $\text{Fe}(\text{NO}_3)_3$ exposure; 59.45 ± 6.20 and $91.44 \pm 6.00\%$ mass, respectively. Similarly, the ^{28}Ni level in the plant treated with the combination of both metals was lower than the single $\text{Ni}(\text{NO}_3)_2$ exposure; 34.41 ± 6.27 and $83.45 \pm 3.43\%$ mass, respectively. It is possible that nickel and iron ions share the same route of transport and translocation, thus the levels of iron and nickel in the roots exposed to the single metal solution are higher than those exposed to the combination of both metal solutions (Ghasemi et al., 2009). Nickel and iron ions share the same loading and transport processes, including transmembrane proteins for active transport (IRT and YSLs) and primary chelators responsible for the metal mobility in plants (NA and citrate) (Nishida et al., 2011).

It was also noted that the significantly reduced levels of ^{17}Cl , ^{19}K , and ^{20}Ca were detected in each metal-treated samples as compared with the control. The levels of ^{17}Cl in the control, Fe-treated, Ni-treated, and Fe/Ni-treated samples were 10.40 ± 1.70 , 0.03 ± 0.04 , 0.83 ± 1.71 , and $0.04 \pm 0.06\%$ mass, respectively. Those of ^{19}K were 36.72 ± 7.85 , 0.01 ± 0.04 , 1.88 ± 2.26 , and $0.17 \pm 0.15\%$ mass, respectively. Those of ^{20}Ca were 28.49 ± 8.50 , 2.01 ± 0.49 , 4.63 ± 0.70 , and $1.00 \pm 0.15\%$ mass, respectively. The reduced levels of these metal ions in the cells were reported as the toxicity effects of Fe and Ni ions via the oxidative stress that caused lipid peroxidation, membrane dismantling, and finally ion leakage (Hossain et al., 2012).



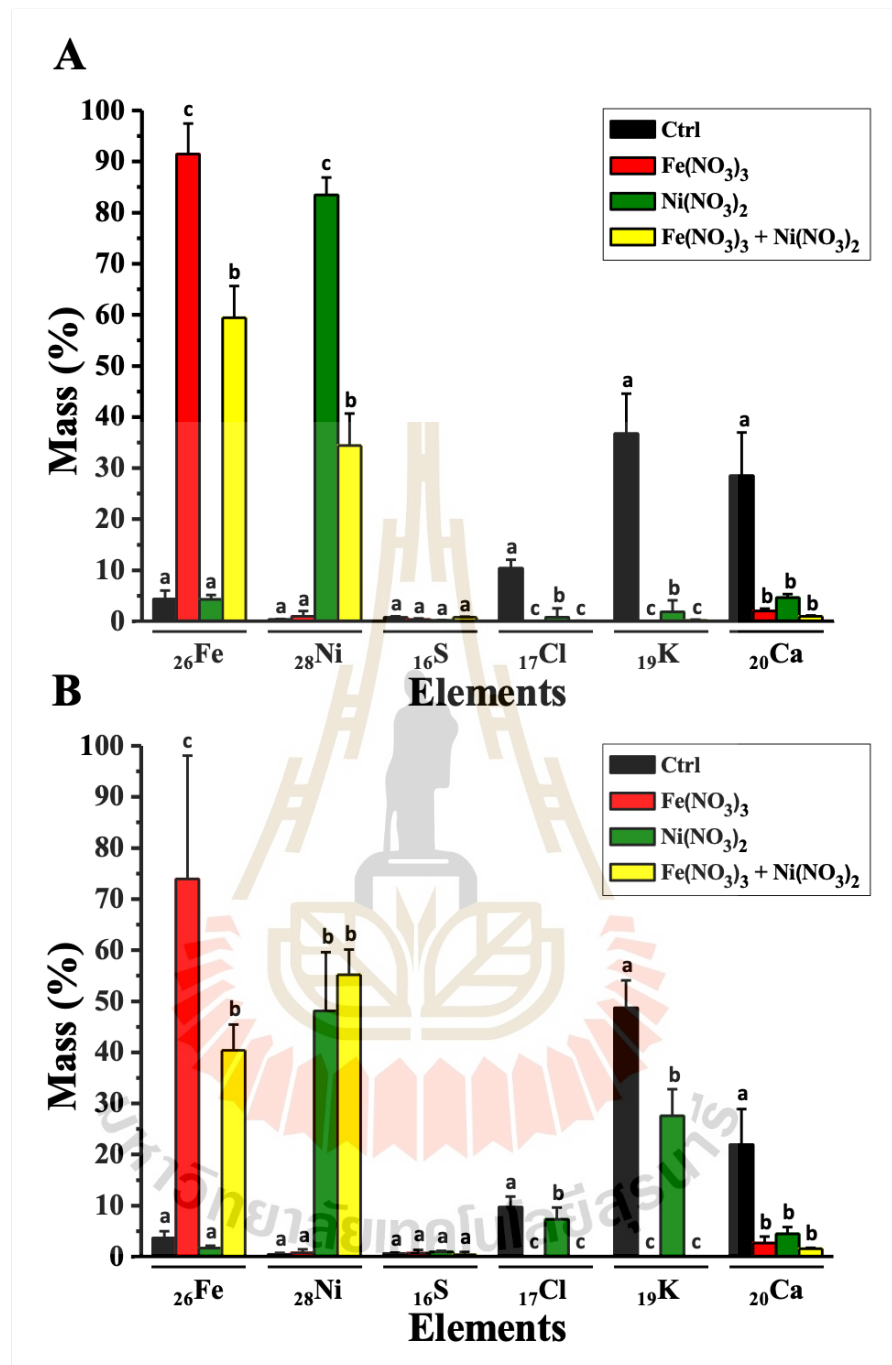


Figure 4.4 XRF quantitative analysis of roots (A) and shoots (B) of metal-treated *Azolla pinnata* R.Br.

Several pieces of research reported the depletion of potassium and calcium caused by the iron and nickel toxicity. Both iron and nickel could induce deficiency of other

macronutrients and micronutrients, such as N, K, Zn, Mn, Ca and Cu, by interfering with their uptakes (Ahmad et al., 2011; Baruah and Bharali, 2015; Brune and Dietz, 1995). The toxicity of iron and nickel partially caused by the induction of ROS, which could cause the oxidative damage of cell membranes and other biomolecules, leading to the leakages of ions from the root cell (Hossain et al., 2012; Piechalak et al., 2005). Therefore, the changes of cellular potassium and calcium ions in *A. pinnata* R.Br. roots and leaves were probably due to their leakages from the injured membranes.

In shoots, similar results were observed, in which *A. pinnata* R.Br. treated with the combination of $\text{Fe}(\text{NO}_3)_3$ and $\text{Ni}(\text{NO}_3)_2$ had the lower level of ^{56}Fe than the single exposure; 40.37 ± 5.09 and $73.94 \pm 24.13\%$ mass, respectively (Figure 4.4(B)). However, the ^{58}Ni level in the plant treated with the combination of $\text{Fe}(\text{NO}_3)_3$ and $\text{Ni}(\text{NO}_3)_2$ was higher than the single $\text{Ni}(\text{NO}_3)_2$ exposure; 48.14 ± 11.45 and $55.17 \pm 4.93\%$ mass, respectively. The previous literatures reported that in hyperaccumulator plants, nickel was easily loaded into the xylem and could rapidly transport to the shoots (Deng et al., 2018). As the result, the major localization of nickel was found in shoots and leaves, but not in roots (He et al., 2012).

Similar to roots, in shoots, the significant reduction levels of ^{37}Cl , ^{39}K , and ^{40}Ca were detected. The levels of ^{37}Cl in the control, Fe-treated, Ni-treated, and Fe/Ni-treated samples were 9.69 ± 2.10 , 0.00 ± 0.00 , 7.32 ± 2.33 , and $0.03 \pm 0.02\%$ mass, respectively. Those of ^{39}K were 48.68 ± 5.41 , 0.00 ± 0.00 , 27.57 ± 5.25 , and $0.00 \pm 0.00\%$ mass, respectively. Those of ^{40}Ca were 21.95 ± 6.93 , 2.67 ± 1.28 , 4.48 ± 1.35 , and $1.54 \pm 0.20\%$ mass, respectively.

4.3 Accumulation of metal NPs in *Azolla pinnata* R.Br.

The *Azolla* plants were reported for their capability to tolerate and accumulate high heavy metals in their tissues (Bennicelli et al., 2004; Wagner, 1997). However, the fate of the uptake-metal ions inside the cells to convert to metal NPs is still questioned. In this work, TEM images were used to analyze the formation of metal NPs in the root tissues of *A. pinnata* R.Br. treated with $\text{Fe}(\text{NO}_3)_3$, $\text{Ni}(\text{NO}_3)_2$, and both solutions.

4.3.1 Cortical cells

In cortical cells, the accumulation of FeNPs was apparently detected at the cell membrane of Fe-treated and both metal-treated root cells (Figure 4.5). In the Fe-treated cells, dispersive FeNPs were dominantly detected in a vicinity of the cell membrane, whereas the additional vacuoles and multivesicular bodies (MVBs) were detected in the cells treated with both $\text{Fe}(\text{NO}_3)_3$, $\text{Ni}(\text{NO}_3)_2$. In contrast, no observation of NiNPs was detected in the cells treated with $\text{Ni}(\text{NO}_3)_2$. It was noted that the plasmolysis was also observed in the cells treated with both solutions as the shrunken cell membrane was detected.

The formation of FeNPs was hypothesized to occur via two mechanisms; the formation of dispersed metal NPs near the cell membrane and the formation of metal NPs in the storage vacuoles. The formation of FeNPs in the vicinity of cell membrane was hypothesized to occur via the transport of Fe^{2+} ions, reduced from Fe^{3+} to Fe^{2+} by FRO, across cell membranes into the plant cells. The phytochemicals near the cell membrane might reduce Fe^{2+} in the presence of oxygen, thus forming iron oxide seed nuclei. These seed nuclei eventually grew into the stable nanoparticles via the assistance of stabilizing phytochemicals. For the formation of FeNPs in the vacuole, it was hypothesized that Fe^{2+} ions were bound an iron transporters, such as IRT1

transporter, and transported into endosomal compartments and vacuoles, where the NPs were formed inside by some reduced and capped biomolecules (Jeong et al., 2017). As a result, Fe^{3+} ions were sequestered, thus preventing oxidative stress and shoot transportation to harm the plant (Briat et al., 2010).

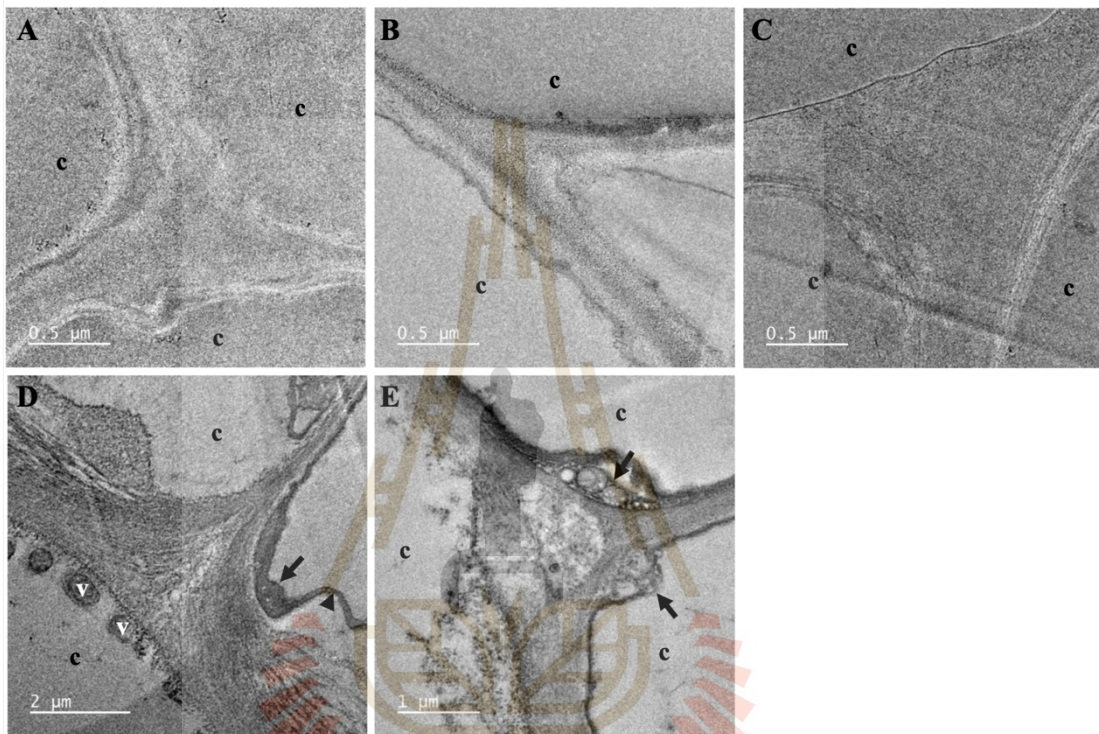


Figure 4.5 TEM images of cortical cells of *Azolla pinnata* R.Br. roots of control (A), $\text{Fe}(\text{NO}_3)_3$ -exposure (B), $\text{Ni}(\text{NO}_3)_2$ -exposure (C), and both metal-exposure (D-E). The letter c is cortical cell, the letter v is vacuoles, the arrows indicate multivesicular bodies, and the arrowhead indicates the plasmolysis.

The detected MVBs, the late endosomes containing membrane-bound intraluminal vesicles, were hypothesized to appear when plants were under attacked by biotic or abiotic stress. Therefore, it was very likely that the formation of MVBs is one

of the important defense mechanisms to iron stress in this work. It was noted that in cortical cells, the detection of these MVBs was only in the condition with both metal treatments. It was hypothesized that nickel ions could interfere the radial transport of Fe ions from the cortical cells to the vasculature (Ghasemi et al., 2009). As the results, very high concentrations of iron ions were in cortical cells, resulting in the formation of MVBs between the cell wall and the plasma membrane of cortical cells.

As vacuoles were also present in Fe-treated cells, it was likely that these vacuoles were formed via the heterotypic fusion between the prevacuolar compartments (PVC)/MVBs to maintain iron in a captured area, thus help to prevent the severe iron toxicity inside the cells (Hu et al., 2020).

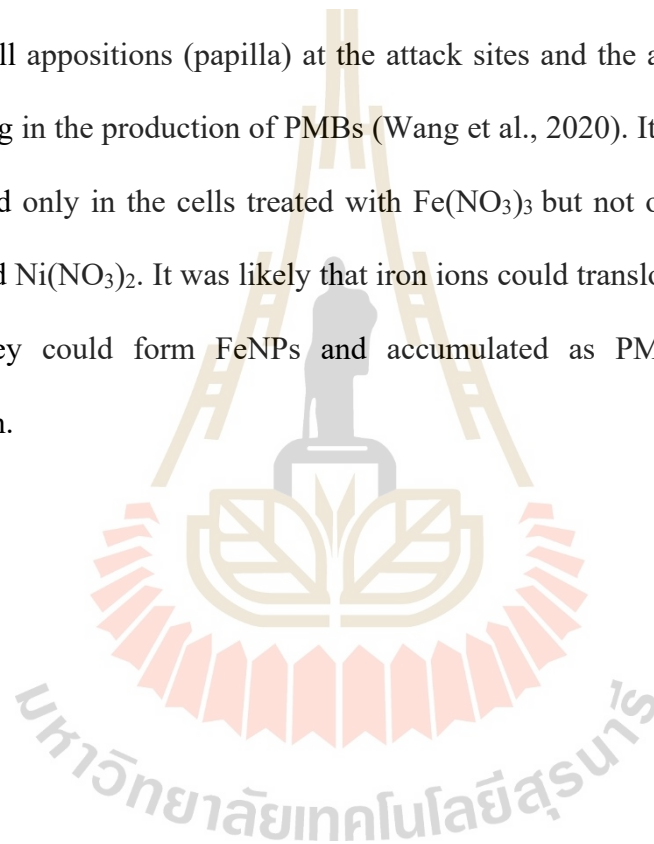
The plasmolysis, the cytoplasmic shrinkage, was existed only in both metal-treated root cells, denoting the cell damage from losing water as the cells were in a hypertonic solution. These cells were known as the plasmolyzed cells (Adamakis and Eleftheriou, 2019).

In this work, it was hypothesized that no formation of NiNPs was likely due to its low accumulated concentration at the root cells. In general, Ni²⁺ ions were specifically bound to intra-cellular chelators, such as NA, His, and organic acids (citric acid and malate ions). Via these chelators, Ni²⁺ ions were transported to shoot and mostly accumulated in the plant leaves (Chen et al., 2009a; Robinson et al., 2003). As the results, this low concentration of Ni²⁺ ions in the root cells was not sufficient to induce the formation of nanoparticles.

4.3.2 Vascular cells

In vascular cells, TEM images of root cells treated with Fe(NO₃)₃, Ni(NO₃)₂, and both metal solutions are shown in Figure 4.6. Similar to the results in cortical cells,

the presence of dispersive FeNPs was detected near the plasma membrane and there was no detected NiNPs. The plasmolysis was also detected in the cells treated both metal ions. Interestingly, the paramural bodies (PMBs; membranous or vesicular structures between cell walls and plasma membranes) were detected in the vascular cells treated with $\text{Fe}(\text{NO}_3)_3$ (Figure 4.6(B)). These PMBs were formed by the fusion between MVBs and the plasma membrane. This mechanism involved the induction of local cell wall appositions (papilla) at the attack sites and the accumulation of metal ions, resulting in the production of PMBs (Wang et al., 2020). It was noted that PMBs were detected only in the cells treated with $\text{Fe}(\text{NO}_3)_3$ but not ones treated with both $\text{Fe}(\text{NO}_3)_3$ and $\text{Ni}(\text{NO}_3)_2$. It was likely that iron ions could translocate to vascular cells, therefore they could form FeNPs and accumulated as PMBs at the sufficient concentration.



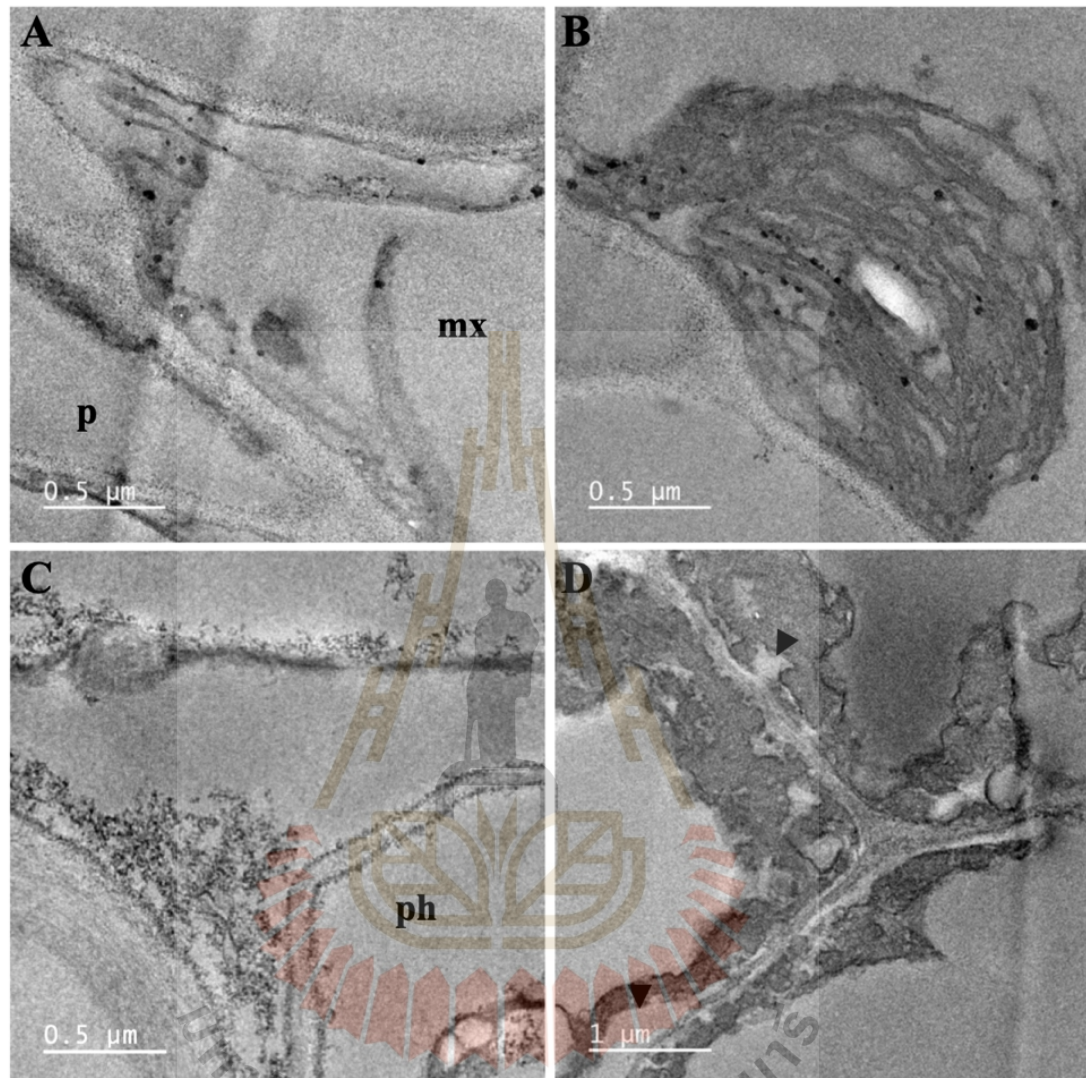


Figure 4.6 TEM images of vascular cells of *Azolla pinnata* R.Br. roots exposed to $\text{Fe}(\text{NO}_3)_3$ (A-B) and the combination of $\text{Fe}(\text{NO}_3)_3$ and $\text{Ni}(\text{NO}_3)_2$ (C-D). The letter p is pericycle, the letter mx is metaxylem, the letter ph is phloem, and the arrowheads indicate the plasmolysis.

4.4 Identity of the metal NPs

The identity of the metal NPs was determined by SEM-EDS and TEM-SAED analyses.

4.4.1 SEM-EDS

SEM-EDS was used to analyze the level of metals in *A. pinnata* R.Br. treated with $\text{Fe}(\text{NO}_3)_3$, $\text{Ni}(\text{NO}_3)_2$, and both metal solutions. The analyses of 92 elements were performed both in roots and shoots of the plants as shown in Figure 4.7.

In roots, SEM-EDS results showed that the untreated *A. pinnata* R.Br. contained two major elements, carbon (C) and oxygen (O), which were the major components of the organic compounds. It was noted that the presence of sodium (Na) was resulted from the sodium phosphate buffer used for the sample preparation. In Fe-treated plants, in addition to C and O, Fe was predominantly detected at 8.90 %wt, suggesting that the plant could uptake Fe ions from the solution into their roots. In Ni-treated plants, a similar result was observed, in which Ni was also detected at 0.20 %wt in addition to C and O. Although the same molar concentrations of $\text{Fe}(\text{NO}_3)_3$ and $\text{Ni}(\text{NO}_3)_2$ were used to treat *A. pinnata* R.Br., the low detection level of Ni as compared with Fe might be resulted from their feasible lost in solution during a sample preparation since Ni mostly in a form of soluble ions, not the membrane-localized, undissolved nanoparticles. In both metal-treated plants, the Fe and Ni were detected in the roots as expected; 7.55 and 0.16 %wt, respectively.

In shoots, the Fe-treated samples contained 0.96 %wt Fe, which was apparently lower than the Fe level in roots. The excessed Fe was typically accumulated in roots as the major sink pool rather than translocated to shoots to prevent the oxidative stress in various vital organelles in leaves. In contrast, the Ni-treated shoots contained

0.56 %wt Ni, which was higher than that in the root, implying that Ni likely preferred to transport and accumulate in shoots more than roots. In both metal ions-treated shoots, the levels of Fe and Ni were at 0.57 and 0.59 %wt. This Fe level was lower than that in roots. In contrast, but this Ni level was higher than that in roots. These results were agreeable with each metal treatment in shoots. Taken together, these results demonstrated the different fates of Fe and Ni ions in uptake, transport, and accumulation in *A. pinnata* R.Br.

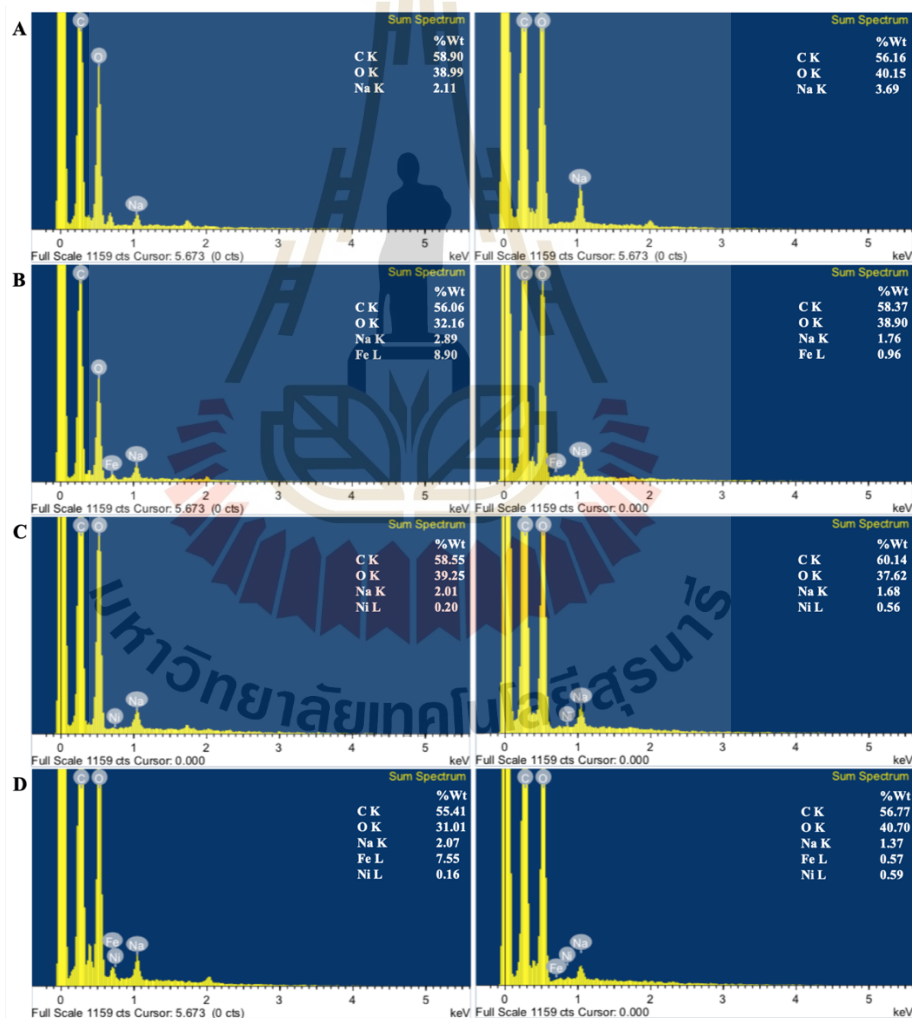


Figure 4.7 SEM-EDS analysis of roots (left) and shoots (right) of *Azolla pinnata* R.Br. under untreated (A), $\text{Fe}(\text{NO}_3)_3$ -treated (B), $\text{Ni}(\text{NO}_3)_2$ -treated (C), both metal-treated (D) conditions.

4.4.1 TEM-SAED

The crystalline structure of the metal NPs in the plant cells was analyzed by TEM-SAED (Figure 4.8). In Fe-treated plants, two forms of FeNPs were detected; Fe₃O₄ (magnetite) and α -Fe₂O₃ (hematite). The detection of the lattice planes at 3.68, 2.66, 2.23, and 1.67 Å suggested the presence of α -Fe₂O₃ (hematite), in which these lattice planes attributed to the hlk planar of α -Fe₂O₃; (012), (104), (113), and (116), respectively. The detection of Fe₃O₄ (magnetite) was indicated by the lattice planes at 4.82, 2.93, and 2.51 Å, corresponding to the hlk planar of (111), (220), and (311) of Fe₃O₄, respectively. Similarly, in Fe- and Ni-treated plants, the concentric diffraction rings of 3.64, 2.23, 1.85, and 1.66 Å were detected, corresponding to the hlk planar of (012), (113), (024), and (116) of α -Fe₂O₃. The concentric diffraction rings of 2.97, 2.54, 2.41, and 1.46 Å corresponded to the hlk planar of (220), (311), (222), and (440) of Fe₃O₄. These analyses were based on the comparisons with the standards JCPDS 01-1053 for Fe₂O₃ (Muraro et al., 2020) and JCPDS No. 01-1111 for Fe₃O₄ (Khaghani et al., 2017). It was noted that SAED analysis revealed no lattice plane of any metal nanoparticles in the plant cells, confirming that there was no formation of NiNPs in these plant cells.

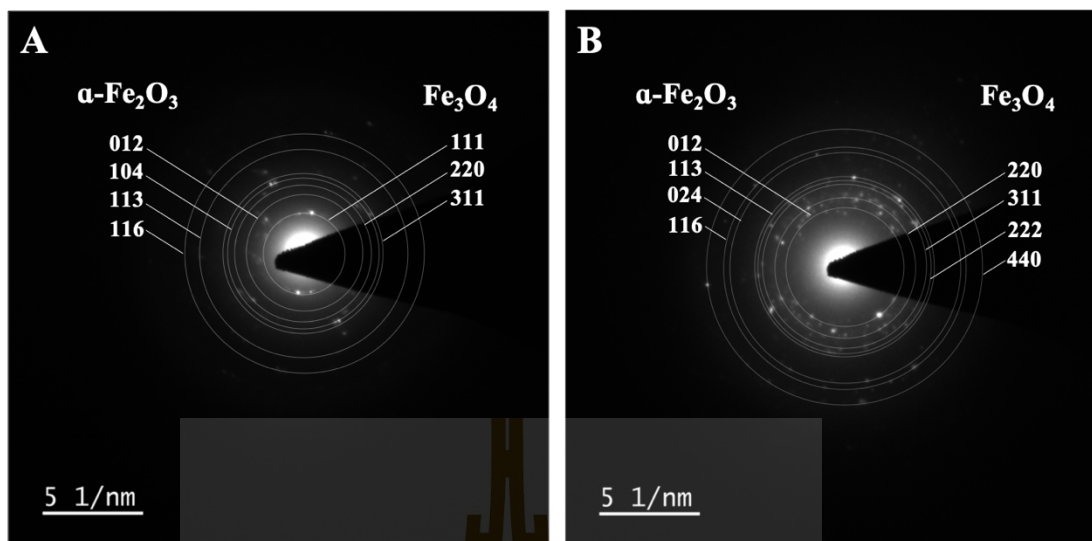


Figure 4.8 SAED-TEM analyses of FeNPs in cortical cells of *Azolla pinnata* R.Br.

roots treated with $\text{Fe}(\text{NO}_3)_3$ (A) and the combination of $\text{Fe}(\text{NO}_3)_3$ and $\text{Ni}(\text{NO}_3)_2$ (B).

4.5 Changes of functional groups of biomolecules

The changes of bio-molecular profiles of *A. pinnata* R.Br. in response to $\text{Fe}(\text{NO}_3)_3$ and $\text{Ni}(\text{NO}_3)_2$ treatments were determined by FTIR spectra in the range of 4000 – 400 cm^{-1} (Figure 4.9).

In roots (Figure 4.9(A)), the FTIR spectra of metal-treated and control plants revealed several differences of functional groups, including peak intensity and appearance of new peaks. In the metal-treated plants, the reduction of peak intensity was detected at 3342–3329, 1057–1032, and 1632–1616 cm^{-1} , which corresponded to the functional groups of O–H stretching of primary alcohol of carbohydrate, C–O (C–C–O) asymmetric stretching of primary alcohol of carbohydrate, and N–H primary amine of protein, respectively (Coates, 2006; Smith, 1998). With the presence of metal ions, these reduced peak-intensities might be attributed to the interaction of divalent

metal ions and O–H functional groups of carbohydrates (i.e. poly-galacturonic acid) in cell wall, thus preventing translocation of metal ions to other parts of the plants (Krzesłowska, 2011). The reduction of C–O stretching might be attributed to a reduction of peroxidation products that was due to a disruption of lipid peroxidation process by metal ions (Lei et al., 2012). A reduction of N–H primary amine suggested the reduction of protein content in the metal-treated *A. pinnata* R.Br., which might be caused by a disruption of newly synthesized protein in metal-stressed cells (Hasan et al., 2017). In addition to the reduced spectral peaks, the increased spectral peaks were detected in the metal-treated *A. pinnata* R.Br. These peaks were detected in the ranges of 1373–1384 and 1243–1232 cm^{-1} , assigning to the symmetrical of carboxyl groups (COO^-) of carbonyl group (Coates, 2006), and antisymmetric of PO_2^- (Garidel et al., 2000). The induction of carbonyl group in metal-treated *A. pinnata* R.Br. might involve a metal detoxification process in plants, such as the induction of pectin to localize and prevent metal translocation via the interaction between metal ions and anion carboxy groups of homogalacturonan domain of pectin (Celus et al., 2018). Also, the induction of phosphate ions suggested the increase of nucleic acids in metal-treated *A. pinnata* R.Br., in which the expression of several genes, especially oxidative and genotoxic relating genes, were induced to facilitate the metal-detoxification process in the cells (Dutta et al., 2018). In the FTIR spectra, two new emerged peaks were detected at 1556–1539 and 672 cm^{-1} , which attributed to N–H bending vibration of amine II and M (Metal)-O bond vibration. The new emergent of amine II peak might be related to a new synthesis of metal stress-related proteins, such as phytochelatins, metallothioneins, and antioxidant enzymes (Kong and Yu, 2007). It was noted that the occurrence of new

M-O bond vibration might support the formation of metal oxide nanoparticles in the plant cells in this work (Doaa et al., 2019; Hamadneh et al., 2019).

In shoots (Figure 4.9(B)), the FTIR profiles were similar to those in roots, in which the reduction and induction peaks were detected. The summary of the FTIR profiles in the roots and shoots was reported in Table 4.1. Three reduction peaks were detected in the ranges of 3337–3291, 1636–1614, and 1030–1025 cm^{-1} , suggesting the reduction of carbohydrates, proteins, and carbohydrates, respectively (Coates, 2006; Smith, 1998). Two induction peaks were detected in the ranges of 1385–1366 and 1517 cm^{-1} , suggesting the induction of carbohydrates and proteins, respectively (Coates, 2006; Kong and Yu, 2007; Smith, 1998). These results suggested the modulation of carbohydrates and proteins in response to metal-treatments. Some induction and reduction of some carbohydrates were reported to involve metal-stress responses in plants; induction of pectin and hemicellulose of cell walls, and reduction of photosynthesis products (glucose and starch) due to the disruption of chlorophyll contents and decrease in the photochemical efficiency of photosystem II by metal ions (Krzesłowska, 2011; S. Singh et al., 2016). Similarly, the modulation of proteins was reported in metal-stressed plants; induction of some metal stress-related antioxidant enzymes and amino acids (citrate, malate, and proline) (Hasan et al., 2017), and disruption/reduction of RuBisCO and other enzymes relating to photosynthetic machinery by metal stress (Hossain and Komatsu, 2013).

Unlike in roots, the FTIR peaks in a range of 1244–1242 cm^{-1} were slightly decreased in the metal-treated samples in the shoots, suggesting the reduced content of nucleic acids. In general, the expression of gene was more active in the shoots than the

roots, therefore the effect of metal ions to suppress gene expression was more obvious in shoots, such as photosynthesis-relating genes (Jaskulak et al., 2018).

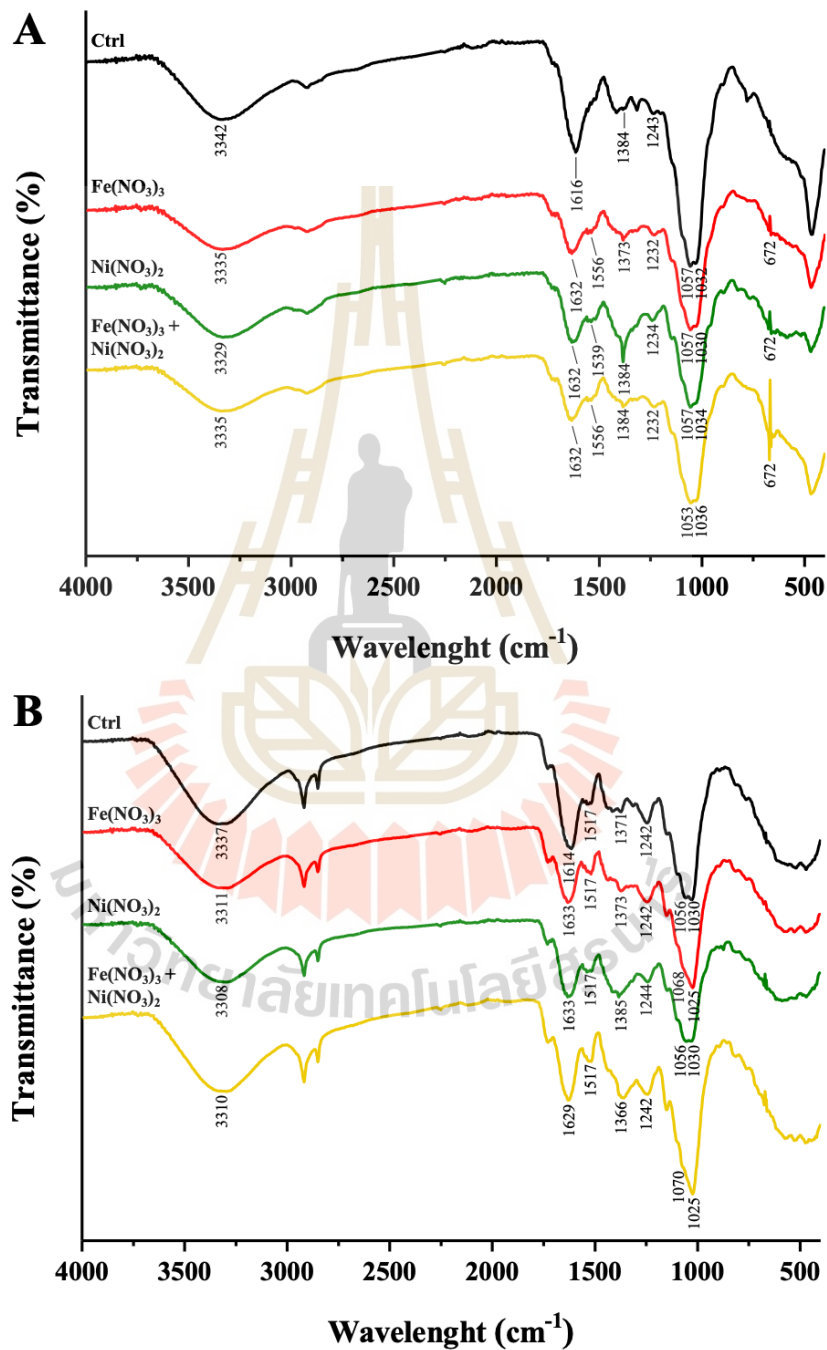


Figure 4.9 FTIR spectra of roots (A) and shoots (B) of *Azolla pinnata* R.Br. in response to metal treatments

Table 4.1 Summary of the FTIR profiles in roots and shoots of *Azolla pinnata* R.Br. in response to metal-treatments.

Biomolecules	Wavelength (cm ⁻¹)	<i>Azolla pinnata</i> R.Br. treated with					
		Roots			Shoots		
		Fe	Ni	Fe/Ni	Fe	Ni	Fe/Ni
Carbohydrates							
O–H stretching	3400–3300	R	R	R	R	R	R
		3335	3329	3335	3311	3308	3310
COO– symmetric stretching	1420–1300	I	I	I	I	I	I
		1373	1384	1384	1373	1385	1366
C–C–O asymmetric stretch of primary alcohols	1070–1000	R	R	R	R	R	-
		1057–	1057–	1053–	1068–	1056–	1070–
		1030	1034	1036	1025	1030	1025
Proteins							
N–H bending of 1° amine	1650–1590	R	R	R	R	R	R
		1632	1632	1632	1635	1636	1634
N–H bending of 2° amide	1575–1480	New	New	New	I	I	I
		1556	1539	1556	1517	1517	1517
Nucleic acids							
antisymmetric PO ₂ ⁻	1260–1215	I	I	I	R	R	R
		1232	1234	1232	1242	1244	1242
Metal–O							
Metal–oxide	500–700	New	New	New	-	-	-
		672	672	672			

Noted: The data were compared with the control. R, Reduction and I, Induction.

4.6 Effect of iron and nickel ions on the oxidative stress enzymes

One of the defense mechanisms of plant cells to metal-stress is the actions of antioxidant enzymes, which major ones are superoxide dismutase (SOD), catalase (CAT), and glutathione reductase (GR) that are related to the reactive oxygen species (ROS) scavenging. SOD is the enzyme to dismutate the superoxide anion ($O_2^{\cdot-}$) to hydrogen peroxide and oxygen. The hydrogen peroxide can be further reduced to water and oxygen by CAT enzyme (Ighodaro and Akinloye, 2018). Also, glutathione peroxidase (GPx) can reduce hydrogen peroxide to water by the redox reaction, which glutathione is also oxidized. The oxidized glutathione can be reversed to its reduced form by GR enzyme. Therefore, the activity of GR indirectly indicates the presence of reactive oxygen species (ROS) (Couto et al., 2016). Therefore, this study evaluated the activities of these enzymes in response to each metal-treatment for the better understanding of the metal-stress responses in *A. pinnata* R.Br.

4.6.1 Roots

In roots (Figure 4.11), the SOD activity was increased in all metal-treated plants as compared with the control plants. The highest SOD activity was detected in the Fe-treated plant, followed by the Fe/Ni-treated, Ni-treated, and control plants, respectively; 264.56 ± 21.02 , 199.78 ± 18.63 , 134.21 ± 19.27 , and 88.83 ± 6.62 U/mg protein. Similarly, the CAT activity was increased in response to metal treatments as compared with the control. The highest CAT activity was detected in the Fe-treated sample, followed by the Fe/Ni-treated, Ni-treated, and control plants, respectively; 88.95 ± 5.23 , 77.00 ± 2.90 , 55.57 ± 3.12 , and 32.93 ± 5.49 nmol min⁻¹ g⁻¹ FW. The results of GR activity were well-agreed with the above enzymes, in which the GR activity was induced in response to all metal-treatments. The highest GR activity was

detected in the Fe-treated sample, followed by the Ni-treated, Fe/Ni-treated, and control plants, respectively; 3.46 ± 0.03 , 2.53 ± 0.03 , 2.58 ± 0.06 , and $2.14 \pm 0.06 \mu\text{mol min}^{-1} \text{g}^{-1} \text{FW}$.

The SOD, CAT, and GR activities indirectly implicated that Fe^{3+} ions induced the most toxicity to *A. pinnata* R.Br. as indicated by the highest activities of these enzymes. It is likely that Fe^{3+} ions are the redox heavy metal, which can generate a high content of ROS via the Fenton/Haber-Weiss reaction. Unlike Fe, Ni is the non-redox heavy metal, which does not directly involve the generation of ROS, but can indirectly induce the activities of some antioxidant enzymes such as SOD, CAT, GPx, GR, and ascorbate peroxidase (APX). The SOD activity was reduced when the plants were treated with Fe/Ni ions as compared with the Fe-treated plants. It might be explained that Ni^{2+} ions could compete the uptake of Fe^{3+} ions (Nishida et al., 2012), resulting in the lower Fe^{3+} uptake as supported by the EDXRF analysis. With the lesser uptake, the SOD activity in the Fe/Ni-treated plants was lower than that in the Fe-treated plants.

4.6.2 Shoots

Similar to the results in roots, the SOD, CAT, and GR activities were induced in response to metal-treatments. Also, the highest enzyme activities were detected in the Fe-treated plant, followed by Fe/Ni-treated, Ni-treated, and control plants. Their SOD activities were 39.79 ± 1.93 , 30.21 ± 3.77 , 28.17 ± 1.37 , and $23.22 \pm 0.43 \text{ U/mg protein}$, respectively. Their CAT activities were 45.35 ± 3.02 , $33.48 \pm 27.71 \pm 0.00$, and $20.12 \pm 3.17 \text{ nmol min}^{-1} \text{g}^{-1} \text{FW}$, respectively. Their GR activities were 2.49 ± 0.26 , 2.33 ± 0.14 , 1.92 ± 0.06 and $1.26 \pm 0.13 \mu\text{mol min}^{-1} \text{g}^{-1} \text{FW}$, respectively. It was noted that the maximal activities of SOD, CAT, and GR in the roots were higher than those

in the shoots. In general, metal ions were mostly accumulated in roots to prevent the translocation of metal ions to other parts of the plants (Ghori et al., 2019). As the results, ROS was more produced in roots than the other parts of the plants.

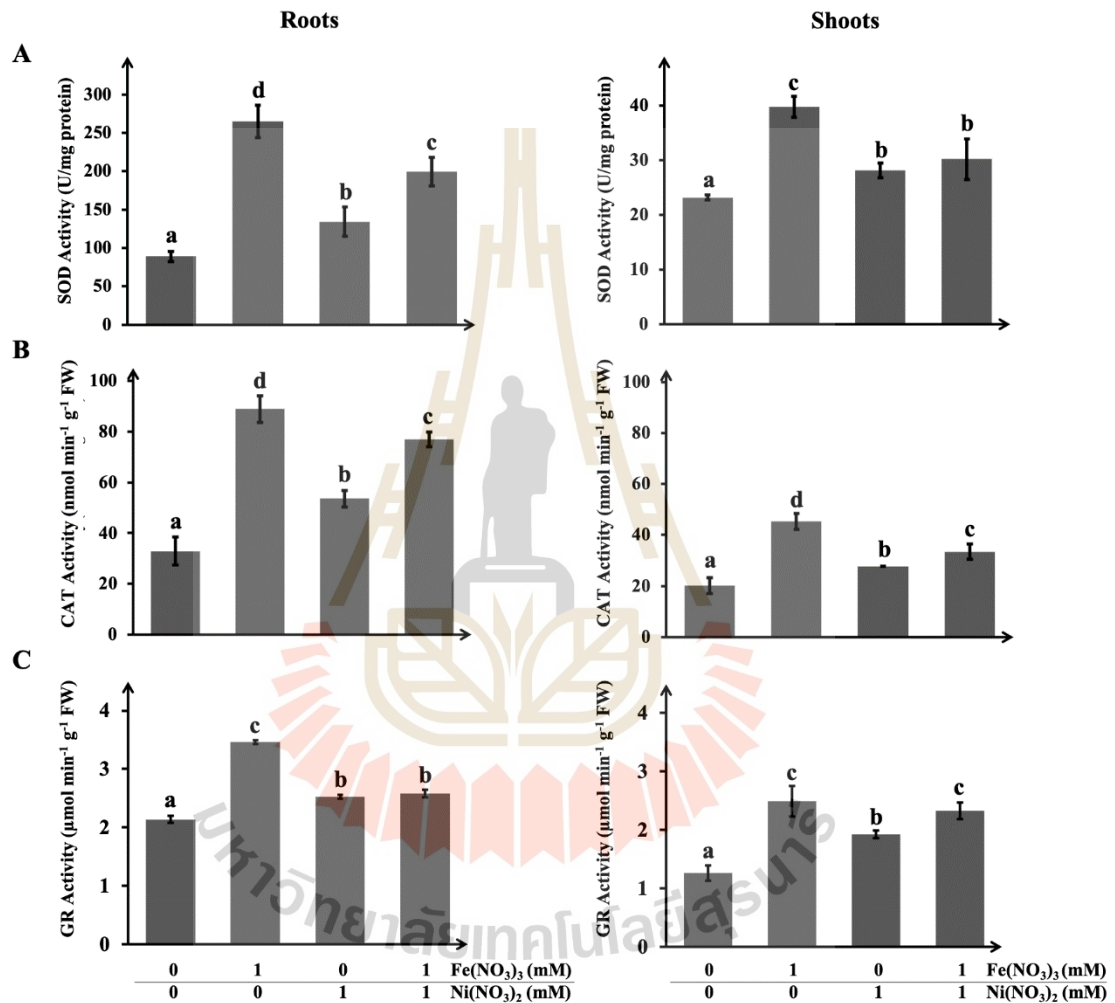


Figure 4.10 The activities of superoxide dismutase (A), catalase (B), glutathione reductase (C) in roots and shoots of *Azolla pinnata* R.Br. treated with Fe(NO₃)₃ and Ni(NO₃)₂.

CHAPTER V

CONCLUSIONS

In this study, the ability of water velvet (*Azolla pinnata* R.Br.), the metal-hyperaccumulator aquatic fern, was investigated for its biosynthesis and the identity of iron and nickel nanoparticles via the uptake Fe^{3+} and Ni^{2+} ions. Also, the metal responses by the plant were investigated; metal-toxicity, metal-uptake (EDXRF), molecular profile (FTIR), and activity of oxidative stress-related enzymes (SOD, CAT, and GR). The conclusion of this study was as follows and the data were also summarized in Table 5.1.

The toxicities of $\text{Fe}(\text{NO}_3)_3$ and $\text{Ni}(\text{NO}_3)_2$ to *A. pinnata* R.Br. were investigated as the plant was treated with single and combination of both solutions, which the results showed that both metals were toxic to the plant in dose-dependence. $\text{Fe}(\text{NO}_3)_3$ was more toxic than $\text{Ni}(\text{NO}_3)_2$, which their 50% toxicity values were 32.61 and 84.33 mM, respectively. Also, the additive toxicity was detected when both metals were used. The uptakes of these metals in the plant were confirmed by EDXRF analysis, which indicated the high contents of both metal ions in roots and shoots, suggesting the uptake and translocation of both metals by this plant. Interestingly, the exposure of both metals resulted in the lower uptake of each metal as compared with the single-metal exposure. This result suggested the competitive uptake between both metals as they shared the same transportation route. The molecular responses to these metals were further investigated by FTIR analysis. The results revealed the induction and reduction of

spectral peak profiles that attributed to function groups of carbohydrates, proteins, and nucleic acids, suggesting the modulation of these macromolecules in *A. pinnata* R.Br. in response to both metals. Also, the FTIR spectral peak indicated the M-O vibration, suggesting the possible formation of metal oxide nanoparticles in the plant cells. In response to these metal exposures, the activities of the antioxidant enzymes (SOD, CAT, and GR) were also investigated. The activities of SOD, CAT, and GR were the highest in the Fe-treated plants, followed by Fe/Ni-treated and Ni-treated plants. These results implied the formation of ROS in response to metal exposures in this plant. Also, since Fe ions were redox-active, it could generate a high content of ROS via the Fenton/Haber-Weiss reaction, resulting in the induction of higher activities of SOD, CAT, and GR in the plant.

The formation of metal nanoparticles was identified by TEM images of the metal-treated plants. Interestingly, only the formation of iron nanoparticles (FeNPs) was detected, but not nickel nanoparticles (NiNPs). The identity of FeNPs was confirmed by TEM-SAED analysis, which indicated hematite (α -Fe₂O₃) and magnetite (Fe₃O₄) forms of FeNPs. FeNPs was accumulated in vesicles and multivesicular bodies, or individually distributed in a vicinity of the cell membranes of cortical and vascular cells. Since the formation of NiNPs was not detected, SEM-EDS analysis was carried out to detect the content of Ni element in the roots. The result showed the low Ni mass in the plant roots, thus suggesting that the low Ni level was insufficient to induce a formation of NiNPs in the plant roots.

In this work, the formation of FeNPs were detected, either the accumulation in the distribution near cell membrane or late endosome and storage vacuole of cortical and vascular cells (Figure 5.1). For the distribution of FeNPs near the cell membrane, it was

hypothesized that some Fe^{2+} ions that entered the cell could be reduced to iron oxide seed nuclei. Then, the metal atoms were continuously aggregated to the seed nuclei and increased the particle size. The particles might be capped with some biomolecules in plant cells to stabilize the formed nanoparticles (Geonmonond et al., 2018). For the formation of FeNPs in late endosomes and vacuoles, it was hypothesized that the excess Fe^{2+} ions were bound to iron transporters at the cell membrane and transported into the endosomal compartments (MVBs and PMBs) and storage vacuoles, where the NPs were formed inside by some reduced and capped biomolecules.

Taken these results together, this work demonstrated the potential cellular production of iron oxide NPs from the uptake iron ions by water velvet, suggesting that this plant species is not only a metal bioremediation plant, which could remove the toxic heavy metal ions from the environment, but also a cellular factory for the production of iron oxide NPs from that contaminated heavy metal ions.

For the future study, these cellular iron oxide NPs have to be isolated from the plant cells, which calcination and chemical cell-lysis methods are proposed (Lee et al., 2017; Yew et al., 2020). Isolation and purification of iron oxide NPs can easily be carried out as they can be trapped by the external magnets. Their physical and chemical properties should be studied, for instance superparamagnetic behavior, catalytic properties, charge, solution stability, and zeta potential (Belanova et al., 2018; Shifrina and Bronstein, 2018). Finally, their potential applications should be investigated such as catalyst, water remediation agent (heavy metal ion removal), magnetic storage, and biomedical material (Yew et al., 2020).

Based on this study, the formation of NiNPs was not detected, which was hypothesized to relate to the insufficient concentration of Ni^{2+} ions. To answer this

question, the formation of NiNPs under different concentrations of Ni^{2+} ions should be investigated, both in roots and shoots. As there was a report of the primary accumulation sites of nickel in newly formed leaves (Page and Feller, 2015), the young leaves should be included in this experiment. In addition, different zones of roots (division, elongation, and maturation zones) should be compared for the formation of NiNPs.



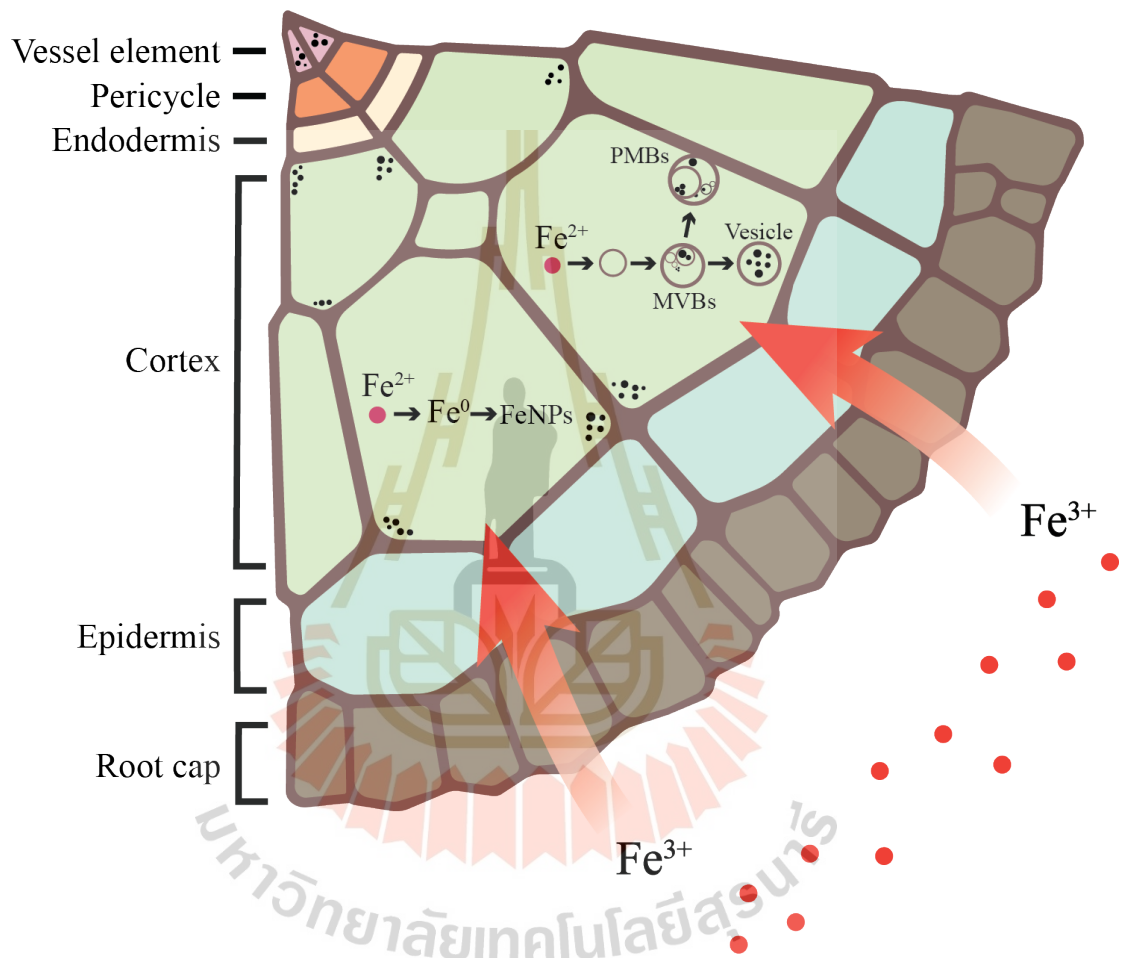


Figure 5.1 Proposed mechanism of the formation of FeNPs in *Azolla pinnata* R.Br.

Table 5.1 Summary of the results.

Experiments	Control	Fe-treated	Ni-treated	Fe/Ni-treated	
Toxicity	TC 50 (mM)				
	–	32.61	84.33	–	
Elemental mass (EDXRF)	% mass				
Roots	²⁶ Fe	4.33 ± 1.70	91.44 ± 6.00	4.27 ± 0.90	59.45 ± 6.20
	²⁸ Ni	0.32 ± 0.16	1.01 ± 1.05	83.45 ± 3.43	34.41 ± 6.27
Shoots	²⁶ Fe	3.68 ± 1.31	73.94 ± 24.13	1.70 ± 0.42	40.37 ± 5.09
	²⁸ Ni	0.45 ± 0.32	0.74 ± 0.73	55.17 ± 4.93	48.14 ± 11.45
Biomolecular profiles (FTIR)					
Roots	–	<ul style="list-style-type: none"> ▪ Reduction peaks of carbohydrates and proteins. ▪ Induction peaks of carbohydrates and nucleic acids ▪ New peaks of proteins and Metal-O 			
Shoots	–	<ul style="list-style-type: none"> ▪ Reduction peaks of carbohydrates, proteins, and nucleic acids. ▪ Induction peak of carbohydrates and protein 			
Activities of antioxidant enzymes (SOD, CAT, and GR)					
Roots		<ul style="list-style-type: none"> ▪ Highest activities in Fe-treated followed by Fe/Ni- and Ni-treated 			
Shoots		<ul style="list-style-type: none"> ▪ Highest activities in Fe-treated followed by Fe/Ni- and Ni-treated ▪ Lower activities than roots 			

Table 5.1 Summary of the results. (Continued)

Experiments	Control	Fe-treated	Ni-treated	Fe/Ni-treated	
Formation of metal nanoparticles (TEM)					
	–	- FeNPs in cortical and vesicle cells	–	- FeNPs in cortical and vesicle cells	
		- Distributed and captured in PMBs		- Distributed and captured in MVBs	
Identity of metal nanoparticles (TEM-SAED)					
	–	α -Fe ₂ O ₃ (hematite) and Fe ₃ O ₄ (magnetite)	–	α -Fe ₂ O ₃ (hematite) and Fe ₃ O ₄ (magnetite)	
Elemental composition (SEM-EDS) %wt					
Roots	C	58.90	56.06	58.55	55.41
	O	38.99	32.16	39.25	31.01
	Na	2.11	2.89	2.01	2.07
	Fe	–	8.90	–	7.55
	Ni	–	–	0.20	0.16
Shoots	C	56.16	58.37	60.14	56.77
	O	40.15	38.90	37.62	40.70
	Na	3.69	1.76	1.68	1.37
	Fe	–	0.96	–	0.57
	Ni	–	–	0.56	0.59



REFERENCES

มหาวิทยาลัยเทคโนโลยีสุรนารี

REFERENCES

- Adamakis, I.-D. S., and Eleftheriou, E. P. (2019). Structural evidence of programmed cell death induction by tungsten in root tip cells of *Pisum sativum*. **Plants (Basel)**. 8(3): 62.
- Aebi, H. (1984). Catalase in vitro. In: **Methods in Enzymology**. Elsevier, pp. 121-126.
- Ahmad, I. Z., Ahmad, A., Mabood, A., and Tabassum, H. (2017). Effects of different metal stresses on the antioxidant defense systems of medicinal plants. In: **Reactive Oxygen Species and Antioxidant Systems in Plants: Role and Regulation under Abiotic Stress**. Singapore, Springer Singapore, pp. 215-256.
- Ahmad, M. S. A., and Ashraf, M. (2011). Essential roles and hazardous effects of nickel in plants. In: **Reviews of Environmental Contamination and Toxicology**. New York, Springer New York, pp. 125-167.
- Ahmad, M. S. A., Ashraf, M., and Hussain, M. (2011). Phytotoxic effects of nickel on yield and concentration of macro- and micro-nutrients in sunflower (*Helianthus annuus* L.) achenes. **Journal of Hazardous Materials**. 185(2): 1295-1303.
- Akbarzadeh, A., Samiei, M., and Davaran, S. (2012). Magnetic nanoparticles: Preparation, physical properties, and applications in biomedicine. **Nanoscale Research Letters**. 7(1): 144-157.
- Ali, S., Abbas, Z., Rizwan, M., Zaheer, I. E., Yavaş, İ., Ünay, A., Abdel-DAIM, M. M., Bin-Jumah, M., Hasanuzzaman, M., and Kalderis, D. (2020). Application of

- floating aquatic plants in phytoremediation of heavy metals polluted water: A review. **Sustainability**. 12(5): 1927.
- Anjum, N. A., Hasanuzzaman, M., Hossain, M. A., Thangavel, P., Roychoudhury, A., Gill, S. S., Rodrigo, M. A. M., Adam, V., Fujita, M., and Kizek, R. (2015). Jaks of metal/metalloid chelation trade in plants—an overview. **Frontiers in Plant Science**. 6(192): 1-17.
- Baruah, K., and Bharali, A. (2015). Physiological basis of iron toxicity and its management in crops. In: **Recent Advances in Crop Physiology**. New Delhi, Daya Publishing House, pp. 203-224.
- Becker, M., and Asch, F. (2005). Iron toxicity in rice—conditions and management concepts. **Journal of Plant Nutrition and Soil Science**. 168(4): 558-573.
- Belanova, A. A., Gavalas, N., Makarenko, Y. M., Belousova, M. M., Soldatov, A. V., and Zolotukhin, P. V. (2018). Physicochemical properties of magnetic nanoparticles: Implications for biomedical applications in vitro and in vivo. **Oncology Research and Treatment**. 41(3): 139-143.
- Bennicelli, R., Stepniewska, Z., Banach, A., Szajnocha, K., and Ostrowski, J. (2004). The ability of *Azolla caroliniana* to remove heavy metals (Hg(II), Cr(III), Cr(VI)) from municipal waste water. **Chemosphere**. 55(1): 141-146.
- Briat, J.-F., Duc, C., Ravet, K., and Gaymard, F. (2010). Ferritins and iron storage in plants. **Biochimica et Biophysica Acta**. 1800(8): 806-814.
- Brumbarova, T., Bauer, P., and Ivanov, R. (2015). Molecular mechanisms governing *Arabidopsis* iron uptake. **Trends in Plant Science**. 20(2): 124-133.
- Brune, A., and Dietz, K. J. (1995). A comparative analysis of element composition of roots and leaves of barley seedlings grown in the presence of toxic cadmium,

- molybdenum, nickel, and zinc concentrations. **Journal of Plant Nutrition**. 18(4): 853-868.
- Castro-Longoria, E., Trejo-Guillén, K., Vilchis-Nestor, A. R., Avalos-Borja, M., Andrade-Canto, S. B., Leal-Alvarado, D. A., and Santamaría, J. M. (2014). Biosynthesis of lead nanoparticles by the aquatic water fern, *Salvinia minima* Baker, when exposed to high lead concentration. **Colloids and Surfaces B: Biointerfaces**. 114: 277-283.
- Celus, M., Kyomugasho, C., Loey, A. M., Grauwet, T., and Hendrickx, M. E. (2018). Influence of pectin structural properties on interactions with divalent cations and its associated functionalities. **Comprehensive Reviews in Food Science and Food Safety**. 17(6): 1576-1594.
- Chen, C., Huang, D., and Liu, J. (2009a). Functions and toxicity of nickel in plants: Recent advances and future prospects. **CLEAN – Soil, Air, Water**. 37(4-5): 304-313.
- Chen, Y., Luo, X., Yue, G.-H., Luo, X., and Peng, D.-L. (2009b). Synthesis of iron–nickel nanoparticles via a nonaqueous organometallic route. **Materials Chemistry and Physics**. 113(1): 412-416.
- Coates, J. (2006). Interpretation of infrared spectra, a practical approach. **A Practical Approach**: 1-23.
- Conte, S. S., and Walker, E. L. (2011). Transporters contributing to iron trafficking in plants. **Molecular Plant**. 4(3): 464-476.
- Couto, N., Wood, J., and Barber, J. (2016). The role of glutathione reductase and related enzymes on cellular redox homeostasis network. **Free Radical Biology and Medicine**. 95: 27-42.

- Das, K., and Roychoudhury, A. (2014). Reactive oxygen species (ROS) and response of antioxidants as ROS-scavengers during environmental stress in plants. **Frontiers in Environmental Science**. 2(53): 1-13.
- Deng, T.-H.-B., van der Ent, A., Tang, Y.-T., Sterckeman, T., Echevarria, G., Morel, J.-L., and Qiu, R.-L. (2018). Nickel hyperaccumulation mechanisms: A review on the current state of knowledge. **Plant and Soil**. 423(1): 1-11.
- Doaa, A. A., Emad, E. E.-K., and Ensaf Aboul, K. (2019). Sol-gel sonochemical triton X-100 templated synthesis of Fe₂O₃/ZnO nanocomposites toward developing photocatalytic degradation of organic pollutants. **Zeitschrift für Physikalische Chemie**: 1-25.
- Dutta, S., Mitra, M., Agarwal, P., Mahapatra, K., De, S., Sett, U., and Roy, S. (2018). Oxidative and genotoxic damages in plants in response to heavy metal stress and maintenance of genome stability. **Plant Signaling & Behavior**. 13(8): e1460048.
- Gajewska, E., and Skłodowska, M. (2010). Differential effect of equal copper, cadmium and nickel concentration on biochemical reactions in wheat seedlings. **Ecotoxicology and Environmental Safety**. 73(5): 996-1003.
- Gardea-Torresdey, J. L., Parsons, J. G., Gomez, E., Peralta-Videa, J., Troiani, H. E., Santiago, P., and Yacaman, M. J. (2002). Formation and growth of Au nanoparticles inside live Alfalfa plants. **Nano Letters**. 2(4): 397-401.
- Garidel, P., Blume, A., and Hübner, W. (2000). A Fourier transform infrared spectroscopic study of the interaction of alkaline earth cations with the negatively charged phospholipid 1,2-dimyristoyl-sn-glycero-3-phosphoglycerol. **Biochimica et Biophysica Acta**. 1466(1-2): 245-259.

- Geonmonond, R. S., Silva, A. G. M. D., and Camargo, P. H. C. (2018). Controlled synthesis of noble metal nanomaterials: Motivation, principles, and opportunities in nanocatalysis. **Anais da Academia Brasileira de Ciências**. 90: 719-744.
- Ghasemi, R., Ghaderian, S. M., and Krämer, U. (2009). Interference of nickel with copper and iron homeostasis contributes to metal toxicity symptoms in the nickel hyperaccumulator plant *Alyssum inflatum*. **New Phytologist**. 184(3): 566-580.
- Ghori, N. H., Ghori, T., Hayat, M. Q., Imadi, S. R., Gul, A., Altay, V., and Ozturk, M. (2019). Heavy metal stress and responses in plants. **International Journal of Environmental Science and Technology**. 16(3): 1807-1828.
- Gurmen, S., Ebin, B., Stopić, S., and Friedrich, B. (2009). Nanocrystalline spherical iron–nickel (Fe–Ni) alloy particles prepared by ultrasonic spray pyrolysis and hydrogen reduction (USP-HR). **Journal of Alloys and Compounds**. 480(2): 529-533.
- Hamadneh, I., Alhayek, H., Al-Mobydeen, A., Abu Jaber, A., Albuqain, R., Alstotari, S., and Al Dujaili, A. (2019). Green synthesis and characterization of yttrium oxide, copper oxide and barium carbonate nanoparticles using *Azadirachta indica* (the neem tree) fruit aqueous extract. **Egyptian Journal of Chemistry**. 62(4): 573-581.
- Hasan, M. K., Cheng, Y., Kanwar, M. K., Chu, X.-Y., Ahammed, G. J., and Qi, Z.-Y. (2017). Responses of plant proteins to heavy metal stress—a review. **Frontiers in Plant Science**. 8(1492).

- He, S., He, Z., Yang, X., and Baligar, V. C. (2012). Mechanisms of nickel uptake and hyperaccumulation by plants and implications for soil remediation. In: **Advances in Agronomy**. Academic Press, pp. 117-189.
- Hossain, M. A., Piyatida, P., da Silva, J. A. T., and Fujita, M. (2012). Molecular mechanism of heavy metal toxicity and tolerance in plants: Central role of glutathione in detoxification of reactive oxygen species and methylglyoxal and in heavy metal chelation. **Journal of Botany**. 2012: 1-37.
- Hu, S., Li, Y., and Shen, J. (2020). A diverse membrane interaction network for plant multivesicular bodies: Roles in proteins vacuolar delivery and unconventional secretion. **Frontiers in Plant Science**. 11(425): 1-15.
- Ighodaro, O. M., and Akinloye, O. A. (2018). First line defence antioxidants-superoxide dismutase (SOD), catalase (CAT) and glutathione peroxidase (GPX): Their fundamental role in the entire antioxidant defence grid. **Alexandria Journal of Medicine**. 54(4): 287-293.
- Ito, A., Shinkai, M., Honda, H., and Kobayashi, T. (2005). Medical application of functionalized magnetic nanoparticles. **Journal of Bioscience and Bioengineering**. 100(1): 1-11.
- Jain, S., Gujral, G., Jha, N., and Vasudevan, P. (1992). Production of biogas from *Azolla pinnata* R.Br and *Lemna minor* L.: Effect of heavy metal contamination. **Bioresource technology**. 41(3): 273-277.
- Jain, S., Vasudevan, P., and Jha, N. (1989). Removal of some heavy metals from polluted water by aquatic plants: Studies on duckweed and water velvet. **Biological Wastes**. 28(2): 115-126.

- Jain, S. K., Vasudevan, P., and Jha, N. K. (1990). *Azolla pinnata* R.Br. and *Lemna minor* L. for removal of lead and zinc from polluted water. **Water Research**. 24(2): 177-183.
- Jan, S., and Parry, J. A. (2016). Heavy Metal Uptake in Plants. In: **Approaches to Heavy Metal Tolerance in Plants**. Singapore, Springer, pp. 1-18.
- Jaskulak, M., Rorat, A., Grobelak, A., and Kacprzak, M. (2018). Antioxidative enzymes and expression of *rbcL* gene as tools to monitor heavy metal-related stress in plants. **Journal of Environmental Management**. 218: 71-78.
- Jeong, J., and Connolly, E. L. (2009). Iron uptake mechanisms in plants: Functions of the FRO family of ferric reductases. **Plant Science**. 176(6): 709-714.
- Jeong, J., Merkovich, A., Clyne, M., and Connolly, E. L. (2017). Directing iron transport in dicots: Regulation of iron acquisition and translocation. **Current Opinion in Plant Biology**. 39: 106-113.
- Khaghani, S., Ghanbari, D., and Khaghani, S. (2017). Green synthesis of iron oxide-palladium nanocomposites by pepper extract and its application in removing of colored pollutants from water. **Journal of Nanostructures**. 7(3): 175-182.
- Khosravi, M., and Rakhshae, R. (2005). Biosorption of Pb, Cd, Cu and Zn from the wastewater by treated *Azolla filiculoides* with H₂O₂/MgCl₂. **International Journal of Environmental Science & Technology**. 1(4): 265-271.
- Kim, E. B., Seo, J. M., Kim, G. W., Lee, S. Y., and Park, T. J. (2016). *In vivo* synthesis of europium selenide nanoparticles and related cytotoxicity evaluation of human cells. **Enzyme and Microbial Technology**. 95: 201-208.
- Kobayashi, T., and Nishizawa, N. K. (2012). Iron uptake, translocation, and regulation in higher plants. **Annual Review of Plant Biology**. 63(1): 131-152.

- Kong, J., and Yu, S. (2007). Fourier transform infrared spectroscopic analysis of protein secondary structures. **Acta Biochimica et Biophysica Sinica**. 39(8): 549-559.
- Krzesłowska, M. (2011). The cell wall in plant cell response to trace metals: Polysaccharide remodeling and its role in defense strategy. **Acta Physiologiae Plantarum**. 33(1): 35-51.
- Küpper, H., and Andresen, E. (2016). Mechanisms of metal toxicity in plants. **Metalomics**. 8(3): 269-285.
- Lal, N. (2017). An overview of nickel (Ni^{2+}) essentiality, toxicity and tolerance strategies in plants. **Asian Journal of Biology**. 2(4): 1-15.
- Laurent, S., Forge, D., Port, M., Roch, A., Robic, C., Vander Elst, L., and Muller, R. N. (2008). Magnetic iron oxide nanoparticles: Synthesis, stabilization, vectorization, physicochemical characterizations, and biological applications. **Chemical Reviews**. 108(6): 2064-2110.
- Lee, S. Y., Cho, J. M., Chang, Y. K., and Oh, Y.-K. (2017). Cell disruption and lipid extraction for microalgal biorefineries: A review. **Bioresource technology**. 244: 1317-1328.
- Lei, J., Xue, S.-g., Wu, C., Wang, J., and Hu, B. (2012). Manganese stress on chemical composition of *Chenopodium ambrosioides* L. by FTIR spectroscopy. **2012 International Conference on Biomedical Engineering and Biotechnology**: 1545-1548.
- Lovley, D. R., Stolz, J. F., Nord Jr, G. L., and Phillips, E. J. P. (1987). Anaerobic production of magnetite by a dissimilatory iron-reducing microorganism. **Nature**. 330(6145): 252-254.

- Lu, A.-H., Salabas, E. L., and Schüth, F. (2007). Magnetic nanoparticles: Synthesis, protection, functionalization, and application. **Angewandte Chemie International Edition**. 46(8): 1222-1244.
- Manara, A. (2012). Plant responses to heavy metal toxicity. In: **Plants and Heavy Metals**. Dordrecht, Springer Netherlands, pp. 27-53.
- Marchiol, L., Mattiello, A., Pošćić, F., Giordano, C., and Musetti, R. (2014). In vivo synthesis of nanomaterials in plants: Location of silver nanoparticles and plant metabolism. **Nanoscale Research Letters**. 9(1): 101.
- Mody, V. V., Cox, A., Shah, S., Singh, A., Bevins, W., and Parihar, H. (2013). Magnetic nanoparticle drug delivery systems for targeting tumor. **Applied Nanoscience**. 4(4): 385-392.
- Moustafa, S. F., and Daoush, W. M. (2007). Synthesis of nano-sized Fe–Ni powder by chemical process for magnetic applications. **Journal of Materials Processing Technology**. 181(1-3): 59-63.
- Müller, C., Kuki, K. N., Pinheiro, D. T., de Souza, L. R., Siqueira Silva, A. I., Loureiro, M. E., Oliva, M. A., and Almeida, A. M. (2015). Differential physiological responses in rice upon exposure to excess distinct iron forms. **Plant and Soil**. 391(1): 123-138.
- Muraro, P. C. L., Mortari, S. R., Vizzotto, B. S., Chuy, G., dos Santos, C., Brum, L. F. W., and da Silva, W. L. (2020). Iron oxide nanocatalyst with titanium and silver nanoparticles: Synthesis, characterization and photocatalytic activity on the degradation of Rhodamine B dye. **Scientific Reports**. 10(1): 3055.

- Nishida, S., Aisu, A., and Mizuno, T. (2012). Induction of *IRT1* by the nickel-induced iron-deficient response in *Arabidopsis*. **Plant Signaling & Behavior**. 7(3): 329-331.
- Nishida, S., Tsuzuki, C., Kato, A., Aisu, A., Yoshida, J., and Mizuno, T. (2011). AtIRT1, the primary iron uptake transporter in the root, mediates excess nickel accumulation in *Arabidopsis thaliana*. **Plant and Cell Physiology**. 52(8): 1433-1442.
- Onyango, D. A., Entila, F., Dida, M. M., Ismail, A. M., and Drame, K. N. (2019). Mechanistic understanding of iron toxicity tolerance in contrasting rice varieties from Africa: 1. Morpho-physiological and biochemical responses. **Functional Plant Biology**. 46(1): 93-105.
- Oren Benaroya, R., Tzin, V., Tel-Or, E., and Zamski, E. (2004). Lead accumulation in the aquatic fern *Azolla filiculoides*. **Plant Physiol Biochem**. 42(7-8): 639-645.
- Page, V., and Feller, U. (2015). Heavy metals in crop plants: Transport and redistribution processes on the whole plant level. **Agronomy**. 5(3): 447-463.
- Park, T. J., Lee, S. Y., Heo, N. S., and Seo, T. S. (2010). *In vivo* synthesis of diverse metal nanoparticles by recombinant *Escherichia coli*. **Angewandte Chemie International Edition**. 49(39): 7019-7024.
- Pattanayak, M., and Nayak, P. (2013). Ecofriendly green synthesis of iron nanoparticles from various plants and spices extract. **International Journal of Plant, Animal and Environmental Sciences**. 3(1): 68-78.
- Peng, C., Wang, X., Chen, J., Jiao, R., Wang, L., Li, Y. M., Zuo, Y., Liu, Y., Lei, L., Ma, K. Y., Huang, Y., and Chen, Z.-Y. (2014). Biology of ageing and role of dietary antioxidants. **BioMed Research International**. 2014: 1-13.

- Piechalak, A., Kozka, M., Malecka, A., Wasinkiewicz, K., Tomaszewska, B., and Baralkiewicz, D. (2005). Influence of lead and cadmium ions on intensity of biosynthesis of phytochelatins in *Pisum sativum* plants. **Chemia i Inżynieria Ekologiczna**. 12(8): 847-851.
- Qin, X. Y., Lee, J. S., Nam, J. G., and Kim, B. S. (1999). Synthesis and microstructural characterization of nanostructured γ -Ni-Fe powder. **Nanostructured Materials**. 11(3): 383-397.
- Rai, P. K. (2007). Wastewater management through biomass of *Azolla pinnata*: An eco-sustainable approach. **AMBIO: A Journal of the Human Environment**. 36(5): 426-428.
- Reddy, L. H., Arias, J. L., Nicolas, J., and Couvreur, P. (2012). Magnetic nanoparticles: Design and characterization, toxicity and biocompatibility, pharmaceutical and biomedical applications. **Chemical Reviews**. 112(11): 5818-5878.
- Robinson, B. H., Lombi, E., Zhao, F. J., and McGrath, S. P. (2003). Uptake and distribution of nickel and other metals in the hyperaccumulator *Berkheya coddii*. **New Phytologist**. 158(2): 279-285.
- Rodríguez, N., Menéndez, N., Tornero, J., Amils, R., and de la Fuente, V. (2005). Internal iron biomineralization in *Imperata cylindrica*, a perennial grass: Chemical composition, speciation and plant localization. **New Phytologist**. 165(3): 781-789.
- Sela, M., Tel-Or, E., Fritz, E., and Huttermann, A. (1988). Localization and toxic effects of cadmium, copper, and uranium in *Azolla*. **Plant Physiology**. 88(1): 30-36.

- Shevyakova, N. I., Cheremisina, A. I., and Kuznetsov, V. V. (2011). Phytoremediation potential of *Amaranthus* hybrids: antagonism between nickel and iron and chelating role of polyamines. **Russian Journal of Plant Physiology**. 58(4): 634-642.
- Shifrina, Z. B., and Bronstein, L. M. (2018). Magnetically recoverable catalysts: Beyond magnetic separation. **Frontiers in Chemistry**. 6(298): 1-6.
- Sikirou, M., Saito, K., Dramé, K. N., Saidou, A., Dieng, I., Ahanchédé, A., and Venuprasad, R. (2016). Soil-based screening for iron toxicity tolerance in rice using pots. **Plant Production Science**. 19(4): 489-496.
- Singh, P., Kim, Y.-J., Zhang, D., and Yang, D.-C. (2016). Biological synthesis of nanoparticles from plants and microorganisms. **Trends in Biotechnology**. 34(7): 588-599.
- Smith, B. C. (1998). **Infrared Spectral Interpretation: A Systematic Approach**. CRC Press.
- Smith, I. K., Vierheller, T. L., and Thorne, C. A. (1988). Assay of glutathione reductase in crude tissue homogenates using 5,5'-dithiobis(2-nitrobenzoic acid). **Analytical Biochemistry**. 175(2): 408-413.
- Sood, A., Uniyal, P. L., Prasanna, R., and Ahluwalia, A. S. (2012). Phytoremediation potential of aquatic macrophyte, *Azolla*. **Ambio**. 41(2): 122-137.
- Suman, J., Uhlik, O., Viktorova, J., and Macek, T. (2018). Phytoextraction of Heavy Metals: A Promising Tool for Clean-Up of Polluted Environment? **Frontiers in Plant Science**. 9(1476).

- Szőllősi, R. (2014). Superoxide dismutase (SOD) and abiotic stress tolerance in plants: An overview. In: **Oxidative Damage to Plants**. San Diego, Academic Press, pp. 89-129.
- Tang, S. C., and Lo, I. M. (2013). Magnetic nanoparticles: Essential factors for sustainable environmental applications. **Water Research**. 47(8): 2613-2632.
- Tran, Q. H., Nguyen, V. Q., and Le, A.-T. (2013). Silver nanoparticles: Synthesis, properties, toxicology, applications and perspectives. **Advances in Natural Sciences: Nanoscience and Nanotechnology**. 4(3): 033001.
- Wagner, G. M. (1997). *Azolla*: A review of its biology and utilization. **The Botanical Review**. 63(1): 1-26.
- Wang, M., Li, X., Luo, S., Fan, B., Zhu, C., and Chen, Z. (2020). Coordination and crosstalk between autophagosome and multivesicular body pathways in plant stress responses. **Cells**. 9(1): 1-19.
- Weng, X., Guo, M., Luo, F., and Chen, Z. (2017). One-step green synthesis of bimetallic Fe/Ni nanoparticles by eucalyptus leaf extract: Biomolecules identification, characterization and catalytic activity. **Chemical Engineering Journal**. 308: 904-911.
- Yew, Y. P., Shameli, K., Miyake, M., Ahmad Khairudin, N. B. B., Mohamad, S. E. B., Naiki, T., and Lee, K. X. (2020). Green biosynthesis of superparamagnetic magnetite Fe₃O₄ nanoparticles and biomedical applications in targeted anticancer drug delivery system: A review. **Arabian Journal of Chemistry**. 13(1): 2287-2308.

Yusuf, M., Fariduddin, Q., Hayat, S., and Ahmad, A. (2011). Nickel: An overview of uptake, essentiality and toxicity in plants. **Bulletin of Environmental Contamination and Toxicology**. 86(1): 1-17.

Zhang, C., Vali, H., Romaner, C. S., Phelps, T. J., and Liu, S. V. (1998). Formation of single-domain magnetite by a thermophilic bacterium. **American Mineralogist**. 83(11-12): 1409-1418.



CURRICULUM VITAE

Name Ratima Janthima

Date of Birth June 8, 1994

Place of Birth Surin, Thailand

Education

2016 – 2020

M.Sc. in Environmental Biology
Suranaree University of Technology, Nakhon Ratchasima,
Thailand

2012 – 2016

B.Sc. in Biology (Honors Program, First Class Degree Honor)
Suranaree University of Technology, Nakhon Ratchasima,
Thailand

Publication

Janthima, R., Khamhaengpol, A., and Siri, S. (2017). Egg extract of apple snail for eco-friendly synthesis of silver nanoparticles and their antibacterial activity. **Artificial Cells, Nanomedicine, and Biotechnology**: 1-7.